International Journal of Applied Earth Observation and Geoinformation 11 (2009) 299–316

Contents lists available at ScienceDirect

International Journal of Applied Earth Observation and Geoinformation

journal homepage: www.elsevier.com/locate/jag

A comparative analysis of a fixed thresholding vs. a classification tree approach for operational burn scar detection and mapping

C.C. Kontoes [a,*], H. Poilvé [b,1], G. Florsch [b,1], I. Keramitsoglou [a], S. Paralikidis [a]

[a] Institute for Space Applications and Remote Sensing, National Observatory of Athens, Metaxa & Vassileos Pavlou Str, GR 152 36, Palea Penteli, Athens, Greece
[b] Infoterra SAS, 31 Avenue des Cosmonautes, 31 402 Toulouse Cedex 4, France

ARTICLE INFO

Article history:
Received 16 December 2008
Accepted 16 April 2009

Keywords:
Earth Observation
Burn scar mapping
Wildfires
Fixed thresholding
Decision tree classification
Landsat 5 TM
SPOT XS
RISK-EOS

ABSTRACT

The scope of this paper is to demonstrate, evaluate and compare two burn scar mapping (BSM) approaches developed and applied operationally in the framework of the RISK-EOS service element project within the Global Monitoring for Environment and Security (GMES) program funded by ESA (http://www.risk-eos.com). The first method is the BSM_NOA, a fixed thresholding method using a set of specifically designed and combined image enhancements, whilst the second one is the BSM_ITF, a decision tree classification approach based on a wide range of biophysical parameters. The two methods were deployed and compared in the framework of operational mapping conditions set by RISK-EOS standards, based either on sets of uni- or multi-temporal satellite images acquired by Landsat 5 TM and SPOT 4 HRV. The evaluation of the performance of the two methods showed that either in uni- or multi-temporal acquisition mode, the two methods reach high detection capability rates ranging from 80% to 91%. At the same time, the minimum burnt area detected was of 0.9–1.0 ha, despite the coarser spatial resolution of Landsat 5 TM sensor. Among the advantages of the satellite-based approaches compared to conventional burn scar mapping, are cost-efficiency, repeatability, flexibility, and high spatial and thematic accuracy from local to country level. Following the catastrophic fire season of 2007, burn scar maps were generated using BSM_NOA for the entirety of Greece and BSM_ITF for south France in the framework of the RISK-EOS/GMES Services Element project.

1. Introduction

In southern Europe thousands of hectares of forests and agricultural land as well as houses and infrastructures are destroyed by forest fires every year. Forest fires across the Mediterranean countries burn about half a million of hectares of woodland per year (Report No. 7: Forest Fires in Europe, 2006, Joint Research Centre, Institute for Environment and Sustainability). Only in Greece, almost 200,000 ha of forested land and natural vegetation, including agricultural parcels and houses were totally destroyed during summer 2007. Fig. 1 sums up the yearly reported size of burnt areas in the five southern European member states, namely Greece, Italy, Portugal, Spain, and France from 1980 to 2004. Fig. 2 shows the number of fire occurrences per member state and depicts the extreme case of Greece during the fire period of 2007 compared to other countries and previous years' records.

Knowledge of past fire events and mapping of burn scars and damages allow for a better understanding of risk as well as fire prevention. Moreover, the identification of damaged areas is of outmost importance to forestry services supporting the reforestation and plantation campaigns, as well as the post-fire management and fire fighting preparation activities for the years following the fire event. The landscape destruction caused by forest fires is being monitored from space using Earth Observation satellites. Several studies have shown that remotely sensed imagery acquired in various spatial, spectral and temporal resolutions is an effective means to delineate the burnt areas and to determine the species affected and the degree of damage caused (Sifakis et al., 2004; Quintano et al., 2006). Burn scars can be clearly identified on a variety of satellite image acquisitions like NOAA/AVHRR, Landsat TM and ETM+, MODIS, MERIS, SPOT and IRS (Fung and Jim, 1998; Koutsias, 2000; Koutsias and Karteris, 2000; Rogan and Yool, 2001; Chuvieco et al., 2002; Fraser and Li, 2002; Pu and Gong, 2004; Gong et al., 2006). In practice, satellite based burn scar mapping takes advantage of the distinctive spectral response of burnt vegetation. Whilst healthy, living vegetation reflects near-infrared (NIR) radiation and absorbs red light in the visible (VIS) part of the spectrum, burnt areas reflect comparatively more radiation in the

* Corresponding author. Tel.: +30 210 8109186; fax: +30 210 6138343.
E-mail addresses: kontoes@space.noa.gr (C.C. Kontoes), herve.poilve@infoterra-global.com (H. Poilvé).
[1] Tel.: +33 5 62197493; fax: +33 5 62199781.

0303-2434/$ – see front matter © 2009 Elsevier B.V. All rights reserved.
doi:10.1016/j.jag.2009.04.001

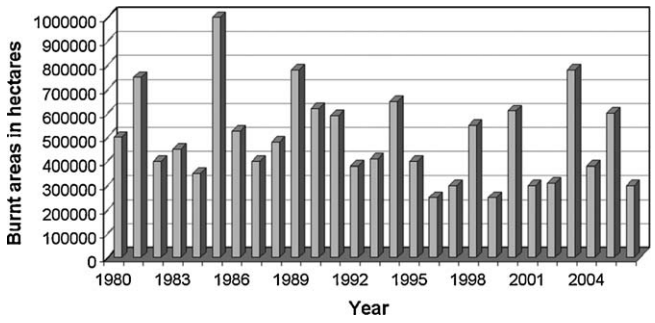

Fig. 1. Yearly reported size of burnt areas in the five southern European member states, i.e. Greece, Italy, Portugal, Spain, and France (source: European Commission, 2006).

VIS and shortwave infrared (SWIR) parts of the spectrum and absorb radiation in the NIR. This is attributed to the destruction of the plant and leaf structure (Rogan and Yool, 2001). Subsequently, elimination of healthy green vegetation and inevitable presence of charcoal or bare soil in the fire zone result in change of radiation recorded by satellite sensors in the relevant spectral bands. These spectral discrepancies between pre- and after-fire image acquisitions allow for a clear identification of the burnt area boundaries.

As far as satellite data processing and automatic fire mapping are concerned, different methods can be employed, the choice being largely dependent on the types of satellite data (spectral, spatial resolution), the area landscape characteristics (mixed land cover classes, fragmented landscape, mixed forests with agriculture) and the size of the study area (region, country, continent). These methods may include fixed thresholding algorithms, adaptive thresholding contextual algorithms (Li et al., 2001) or integration of the two (Gong et al., 2006) applied on image spectral bands and/or computed indices derived from uni- or multi-temporal image acquisitions. The fixed thresholding method applies empirically determined thresholds to discriminate burnt pixels from their non-burnt surroundings. The advantages of the method are simplicity and processing speed. The method can successfully detect burnt area pixels; however, its main limitation is that the specific threshold values need to be adapted to the geographic area as they depend largely on the type of land cover/land use classes as well as their diversity. On the other hand, the adaptive thresholding algorithms compute variable, pixel-specific thresholds based on the geographic context of a pixel (Boles and Verbyla, 2000); however, special attention should be paid to setting the right thresholds for the discrimination of potential burnt pixels.

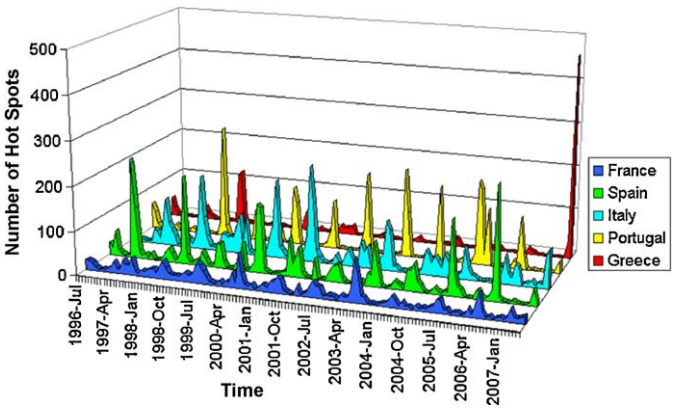

Fig. 2. Number of fire occurrences for each of the five southern member states. The extreme case over Greece during the fire period of 2007 compared to other countries and previous years' records is highlighted (source: The Along Track Scanning Radiometer (ATSR) fire atlas of ESA, 2007, http://www.esa.int.esaEO, credits ESA).

Apart from data thresholding techniques, there exist methods employing logistic regression on uni- or multi-temporal image bands and other image parameters. For instance, image derived indices (e.g. vegetation indices) coupled with geographic data (Koutsias, 2000), methods using linear and/or non-linear spectral mixture analysis techniques (Sa et al., 2003; Ustin, 2004), rule-based tree classification (Simard et al., 2000) and neural network (Pu and Gong, 2004) methods. The flexibility obtained is that continuous data, such as radiances, vegetation indices and topographic data (e.g. Digital Elevation Model, slope data), can be used in conjunction with thematic data, such as land cover/land use data, forest stand data, vegetation density, or ecosystem pressure indicators, for burnt area mapping and damage assessment.

Extraction of burnt land information from remotely sensed data can be performed either by using uni-temporal or multi-temporal image acquisitions. Three different approaches have been reported including, (a) application of multiple tests on spectral values and indices derived from uni-temporal data, (b) multi-temporal change analysis of spectral and biophysical indices, and (c) image segmentation and classification techniques using uni- or multi-temporal data (Arino et al., 1999). In the first approach, the identification of burnt areas is performed by analysing the spectral differences of image bands and image-derived indices (e.g. Normalised Burnt Ratio Index; Key and Benson, 2003) using a single post-fire image (Pereira, 1999). In certain projects this approach is preferred to a mutli-temporal one, as it makes the study competitive and straightforward. In the second approach, the temporal changes of spectral and/or biophysical parameters due to fires are detected using two images, pre- and post-fire (Martin and Chuvieco, 1995; Miller and Yool, 2002; Fisher et al., 2003). Analysing either the post-fire decrease of vegetation vigour (e.g. multi-temporal change analysis of Vegetation Indices), or the changes depicted in a multi-temporal Principal Components Analysis (PCA) vectors (Fisher et al., 2003), or even the changes of brightness, greenness, and wetness components introduced by the so-called Kauth-Thomas Transform (Collins and Woodcock, 1996), the burnt areas can be identified and mapped more effectively than using a single image. In addition, this approach minimises the spectral confusion of burnt areas with other land cover types such as permanent crops, open agricultural fields, shadows, urban and water surfaces. The third method involves conventional image classification and post-classification of uni- or multi-temporal satellite data and image derived indices.

The scope of this research study is to present and evaluate two burn scar mapping methods, developed and applied operationally in the framework of the RISK-EOS service element within the Global Monitoring for Environment and Security (GMES) program funded by ESA (http://www.risk-eos.com). The two methods refer to (a) the so-called BSM_NOA, which is a fixed thresholding method, developed by the Institute for Space Applications and Remote Sensing of the National Observatory of Athens (ISARS/NOA), and (b) the BSM_ITF approach, a decision tree classification approach based on a wide range of biophysical parameters produced by the Overland Thematic Processor software (Overland). The company Infoterra SAS France (ITF) initially developed the Overland tool to address land use/land cover mapping needs. The two methods were standardised, qualified and validated in the framework of the RISK-EOS service element project over Greece and south France, respectively. This paper is the first attempt to compare the two methods following the same standards for burnt/unburned area mapping (i.e. mapping accuracy and thematic representation) according to the RISK-EOS validation protocol. The two methods are evaluated for both uni- and multi-temporal analysis and for different types of input satellite data, as far as the image spectral and spatial resolution properties are concerned.

This research study was undertaken to determine the effectiveness of the two classifiers, considering that different satellite data (in terms of spectral and spatial characteristics) and acquisition modes (single- or multi-date) are selected. It also assesses the performance of the two methods when different image enhancements are applied (e.g. spectral indices vs. biophysical parameters) to meet the requirement for effective and rapid separation of burnt from unburned vegetation in the Greek landscape environment.

2. Operational requirements for burn scar mapping

The major goal of operational burn scar mapping is the timely provision of accurate post-fire information concerning the size and the types of damages, the degree of vegetation recovery and any man-made changes within the affected zones. The service provides support to regional, provincial and national governmental entities in taking actions for fire fighting plans and environmental and natural resources planning, as well as for implementing land use/land cover and soil conservation measures according to the provisions of the existing legal frame. To this end the RISK-EOS fire databases, yearly populated in south European countries with information relating to the position and shape of the fires, is anticipated to assist civil protection and fire fighting organisations in preparing for a potential fire crisis in the future, and in predicting reliably the fire risk. This improves the existing fire prevention capability and fire behaviour knowledge in the area of their authority.

The two methods presented in this study, promote the use of remotely sensed data as an alternative to conventional aerial mapping campaigns and field surveys. This is due to the fact that the visual interpretation of aerial acquisitions and deployment of in-situ GPS surveys have proven to be labour-intensive and time-consuming. In addition, the resultant maps are not as exhaustive and accurate as with the application of the proposed approaches, and this is manifested appropriately in Section 4.

3. Methodological approaches description

3.1. The "BSM_NOA" approach

3.1.1. Overview

BSM_NOA is a fixed thresholding approach developed in the Institute for Space Applications and Remote Sensing of the National Observatory of Athens (ISARS/NOA). It relies on automatic processing tools, using uni- and/or multi-temporal derived spectral indices, as well as on a proprietary radiometric change vector analysis approach suggested by Kontoes (2008). The decision for a uni- or multi-temporal approach depends upon the number of available image acquisitions. The processing chain is divided into three main levels of operations, namely BSM_NOA Pre-processing, BSM_NOA Core Processing and BSM_NOA Quality Control and Photo-interpretation (BSM_NOA post-processing). These are summarised below.

In the *Pre-processing phase* the following tasks are performed:

(a) Satellite data radiometric normalisation.
(b) Satellite data geo-referencing and mosaicking.
(c) Cloud/water/shadow mask generation.
(d) Radiometric change vector calculation and change/no-change mask generation.
(e) Band transformation calculations and spectral indices generation (uni- or multi-temporal).
(f) Definition of appropriate index thresholds using samples of known fires (e.g. sample data available in Regional Forestry Services). The defined thresholds are satellite sensor specific.

During the *Core Processing phase* the thresholded spectral indices are combined to achieve a first separation between burnt and unburned areas. To resolve for remaining ambiguities and enhance the first burn scar mapping output, this map is compared against to the change/no-change pixel map, output of the radiometric vector change analysis. This phase is extensively described in the subsequent Section 3.1.2.

In the *post-processing (refinement) phase*, the order of the tasks is as follows:

(g) Removal of pixel noise from the generated burnt/unburned raster map using a median filter, and elimination of objects smaller than the specified minimum mapping unit (MMU).
(h) Raster-to-vector transformation in order to create burn scar boundaries.
(i) Visual inspection of the resultant burn scar polygons and comparison with the original image data. This step is crucial since burn scar polygon aggregation cleans the map from unnecessary small island polygons and improves the thematic value of the map.
(j) Polygon smoothing and integration of meaningful attribute information for each burn scar polygon such as, polygon surface, polygon perimeter, damage assessment in terms of area per land cover type, place-name, date of fire ignition, date of fire suppression, etc.

3.1.2. The BSM_NOA core processing

As mentioned the BSM_NOA approach applies a fixed thresholding model on uni- or multi-temporal image enhancements. Image enhancements consist of arithmetic combinations of satellite image bands based on sensor spectral characteristics. The method was developed so as to be applicable to a wide range of sensor bands in the visible, near infrared and mid infrared. Its design allows flexibility not only in wavelength selection, but also in the processing of any commercial sensor such as Landsat TM and ETM+, SPOT, IRS/WiFS, IKONOS-2, FORMOSAT-2, MODIS, MERIS, etc. The image enhancements used by the BSM_NOA model for burnt area mapping are described in the following.

3.1.2.1. The Normalised Burn Ratio index (NBR). It is one of the most widely used image enhancements for mapping wildfires worldwide. Key and Benson (2003) introduced this index as a variation of the normalised difference vegetation index (NDVI). They replaced the red reflectance value in the NDVI with the mid-infrared reflectance value:

$$\mathrm{NBR} = \frac{(R_{\mathrm{NIR}} - R_{\mathrm{MIR}})}{R_{\mathrm{NIR}} + R_{\mathrm{MIR}}} \quad (1)$$

Several researchers have proposed this index for burnt area mapping (Cocke et al., 2005; Roy et al., 2006), as reflectance values in the red and mid-infrared exhibit the greatest reflectance change in response to a fire (see also Section 1). Although NBR has been effective in many burnt areas mapping studies, it has not been widely tested in the Greek ecosystems. BSM_NOA uses NBR in combination with other spectral indices for the reasons described hereinafter.

In the south Mediterranean zones and especially within the Greek pine and shrub land ecosystems, the land abandonment has resulted in intense fuel accumulation. Because of this, a significant reduction in green vegetation is reported inside the burnt areas after a fire occurrence. In these areas, the NBR index can differentiate accurately between burnt and unburned areas. Forest ecosystems though, are much diversified in Greece and forest canopy density decreases form north to south. Therefore, the forest stands become less uniform and are interrupted by the presence of agricultural fields, dispersed settlements, roads, open fields,

abandoned farms or permanent crop cover. This high mixture of classes makes automatic image segmentation with the sole use of NBR problematic. Indeed, since the burnt vegetation is characterised by an increase of reflectance in the visible, a decrease in the near infrared and a slight increase in the mid-infrared, the spectral response of burnt forests tends to be more 'flat' than that of healthy vegetation, which may cause confusion with non-vegetation classes like open agricultural fields, bare soils, water surfaces, urban areas or permanent crops. This type of confusion between charcoal and other soil colours in highly fragmented ecosystems was also reported by Rogan and Yool (2001) who suggested the use of the Kauth and Thomas Tasselled Cap Transformation (Kauth and Thomas, 1976) to resolve the reported confusion. In order to cope with this problem the BSM_NOA approach integrates two additional spectral indices complementary to NBR. These two image enhancements are the Normalised Difference Vegetation Index (NDVI) and the so-called empirical Albedo index.

3.1.2.2. The uni- and/or multi-temporal Normalised Difference Vegetation Index (NDVI and $NDVI_{MULTI}$). The NDVI is a common spectral vegetation index derived by dividing the difference between reflectance in the NIR and the visible RED channels by the sum of the two (Rouse et al., 1974):

$$\mathrm{NDVI} = \frac{(R_{\mathrm{NIR}} - R_{\mathrm{RED}})}{R_{\mathrm{NIR}} + R_{\mathrm{RED}}} \quad (2)$$

NDVI has long been used in the Mediterranean for assessing the vegetative health and moisture content of an area and resolve ambiguities in the discrimination between healthy and dead or removed vegetation (Tappan et al., 1992; Marsh et al., 1992; Lyon et al., 1998). Moreover, NDVI has been used to demonstrate the extent of vegetation removal associated with a fire event as it exhibits a sharp post-fire drop (Li et al., 2000; Diaz-Delgado and Pons, 2001; Vafeidis and Drake, 2005). Depending on the number of acquisitions the NDVI analysis can be uni-temporal (calculated only at post-fire level) or multi-temporal. The multi-temporal difference of NDVI adopted in BSM_NOA is denoted as $\mathrm{NDVI}_{\mathrm{multi}}$ and is calculated as in equation 3 below.

$$\mathrm{NDVI}_{\mathrm{MULTI}} = \mathrm{NDVI}_{\mathrm{PRE\text{-}FIRE}} - \mathrm{NDVI}_{\mathrm{POST\text{-}FIRE}} \quad (3)$$

The multi-temporal NDVI approach is preferred to a uni-temporal one, as it better resolves the confusion between classes. Several studies have differenced pre-fire and post-fire NDVI images to discern fire scars fast and efficiently (Cahoon et al., 1992; Kasischke et al., 1993; Kasischke and French, 1995; Li et al., 1997; Leblon et al., 2001).

3.1.2.3. The Albedo Index. In highly diversified Mediterranean ecosystems, the NDVI might put limitations on the detection and delineation of burnt from the unburned surfaces. Pereira (1999) and Elmore et al. (2000), concluded that NDVI is affected by the soil colour and is therefore not always comparable across a heterogeneous area. Due to this, BSM_NOA integrates the empirical approximation of the surface Albedo (Saunders, 1990; Lasaponara, 2006), which is an indicator of the surface brightness. The Albedo index is calculated as in equation 4 below.

$$\mathrm{ALBEDO} = \frac{R_{\mathrm{NIR}} + R_{\mathrm{RED}}}{2} \quad (4)$$

From the above it is shown that none of the proposed image enhancements can, by itself, be considered appropriate to efficiently resolve the problem of burnt area mapping in south Mediterranean ecosystems. For this, the BSM_NOA approach suggests the appropriate thresholding and combined use of the three image enhancements, and the comparison of the resulted burn scar map with a change/no-change pixel layer, generated by a pixel based change vector analysis approach suggested in Kontoes (2008). This approach is presented next.

Let us assume two images of n bands each, one acquired in pre-fire (master image) and the other in post-fire (slave image) seasons respectively. These images may be represented as vectors in the n-dimensional image space, denoted as $\vec{G_1} = (g_{11}, g_{12}, \ldots, g_{1n})^T$ and $\vec{G_2} = (g_{21}, g_{22}, \ldots, g_{2n})^T$.

The change vector $\vec{\Delta G}$ is then defined as: $\vec{\Delta G} = \begin{pmatrix} g_{11} - g_{21} \\ g_{12} - g_{22} \\ \cdots \\ g_{1n} - g_{2n} \end{pmatrix} = \begin{pmatrix} \delta g_1 \\ \delta g_2 \\ \cdots \\ \delta g_n \end{pmatrix}$

Obviously the greater the magnitude of the change vector $\vec{\Delta G}$, the higher the probability of change occurrence between the two images. The accurate and reliable identification of "change" and "no-change" pixels depends on the proper definition of threshold T as far as the change vector magnitude parameter is concerned. T is usually a single value and applies to the entire difference image $\left|\vec{\Delta G}\right| = \sqrt{\delta g_1{}^2 + \delta g_2{}^2 + \ldots + \delta g_n{}^2}$ at pixel level. During processing the change magnitude $\left|\vec{\Delta G}\right|$ is compared with T and the pixel is assigned the "change" or "no-change" label if $\left|\vec{\Delta G}\right|$ is greater or less than T. The greater the difference between $\left|\vec{\Delta G}\right|$ and T, the higher the user confidence in separating the "change" from the "no-change" areas. To efficiently address the problem of change area estimation, the BSM_NOA approach considers evidence derived from pixel's geographic vicinity, the latter being a 3×3 pixels kernel. This can be achieved by calculating the spectral vector differences $|\Delta G_{ij}|$ between any pixel i on the first image and the corresponding nine (3×3 pixels) j ($j = 1$ to 9) located in the immediate neighbourhood of pixel i on the second image. The comparison of the nine $|\Delta G_{ij}|$ values with T gives nine distinct pieces of evidence for pixel i of the type "change" or "no-change". According to the proposed approach, the pixel i is assigned the label "change" if all of the nine bits of evidence associated to this pixel, fully support this decision. In the opposite case, the pixel is defined as "no-change". Furthermore, a measure indicating the degree of confidence to this decision is calculated by the BSM_NOA processing chain and is stored in a separate information layer. This measure is directly linked to the number of occurrences a pixel has been identified as "no-change" based on pixel's changed radiometry. Thus, this value can vary between 1/9 and one. It is then up to the analyst to decide the level of confidence to rely on for identifying the "change" and the "no-change" areas in the studied affected region.

Fig. 3a describes the three phases of the BSM_NOA multi-temporal processing chain based on pre-fire and post-fire image acquisitions to generate burnt scar maps in vector and raster format. Fig. 3b presents the processing steps for "change/no-change" map generation based on pixel's radiometric changes due to fire, as described in Kontoes (2008).

3.2. The "BSM_ITF" approach

3.2.1. Overview

The BSM_ITF method is a decision tree classification approach developed by Infoterra SAS France using the biophysical informa-

tion layers produced from raw image data by proprietary software, the so called Overland Thematic Processor software (Overland). Overland uses a comprehensive set of BRDF (Bidirectional Reflectance Distribution Function) models to simulate vegetation, soil, water, and transmission through the atmosphere, and is able to process data from a whole family of optical sensors having various spectral configurations. The resulting biophysical layers provide absolute physical information that serves as criteria to identify burnt vegetation pixels either from a single image (post-fire, uni-temporal) or from a multi-temporal analysis (pre- and post-fire). This pixel classification is further processed to provide reliable "fire seeds" and then to produce the final map of burnt areas using a region growing process. The overall processing chain is divided in three main steps as follows:

Processing of biophysical information:

(a) Import of geo-corrected images (DN values).
(b) Automatic processing to generate biophysical layers characterising the soil and vegetation conditions. Additional layers relating to water and clouds are produced for masking the corresponding areas.

Pixel classification of burnt vegetation:

(c) Pixel classification based on a decision tree approach exploiting the whole set of biophysical layers. For this, a set of reference decision trees have been set up corresponding to uni- and multi-temporal image analysis. Threshold values are finely tuned using the Overland interactive classification tool.
(d) Export of classification result as a raster map (GeoTIFF format).

Generation of burn scar maps:

(e) Suppression of burnt/unburned raster map pixel noise by considering burnt pixels as fire seeds and filtering out noise according to a threshold for fire seeds local density.
(f) Identification of each individual fire by merging fire seeds within a given distance using a sliding window kernel. Production of a Region Of Interest (ROI) for each detected fire.
(g) Apply a region growing process to each ROI fire until the residual vegetation criterion depicted on the corresponding vegetation biophysical layer reaches a certain threshold.
(h) Visual interpretation of the resultant map and if necessary manual corrections at individual fire ROIs.

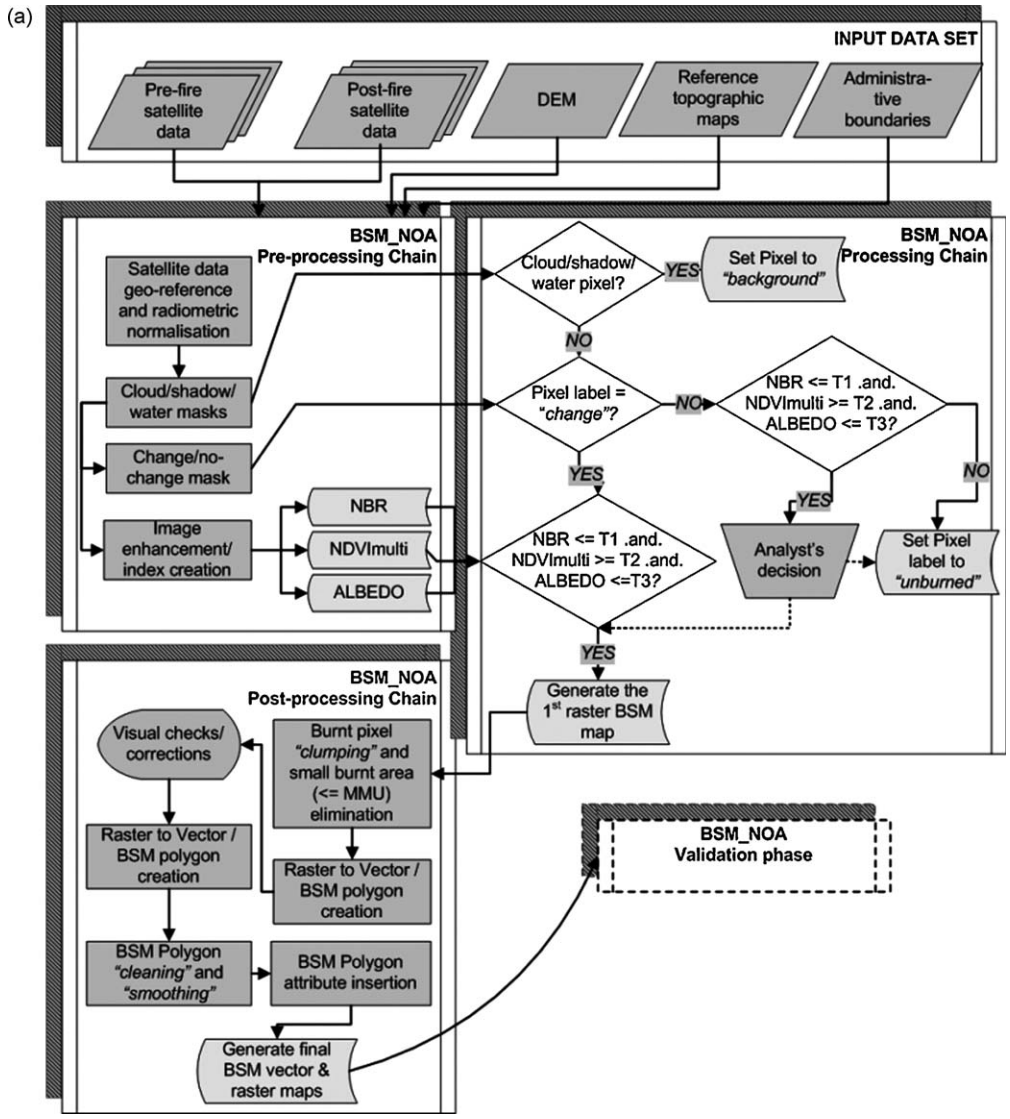

Fig. 3. (a) Flow diagram of the BSM_NOA multi-temporal processing chain. In the case of using Landsat TM data the fixed thresholds which were set over Greece have been, T1 = 126 (0–255), T2 = 0.3 and T3 = 50, (b) Change/no change pixel map resulting from the kernel based thresholding method suggested in Kontoes (2008).

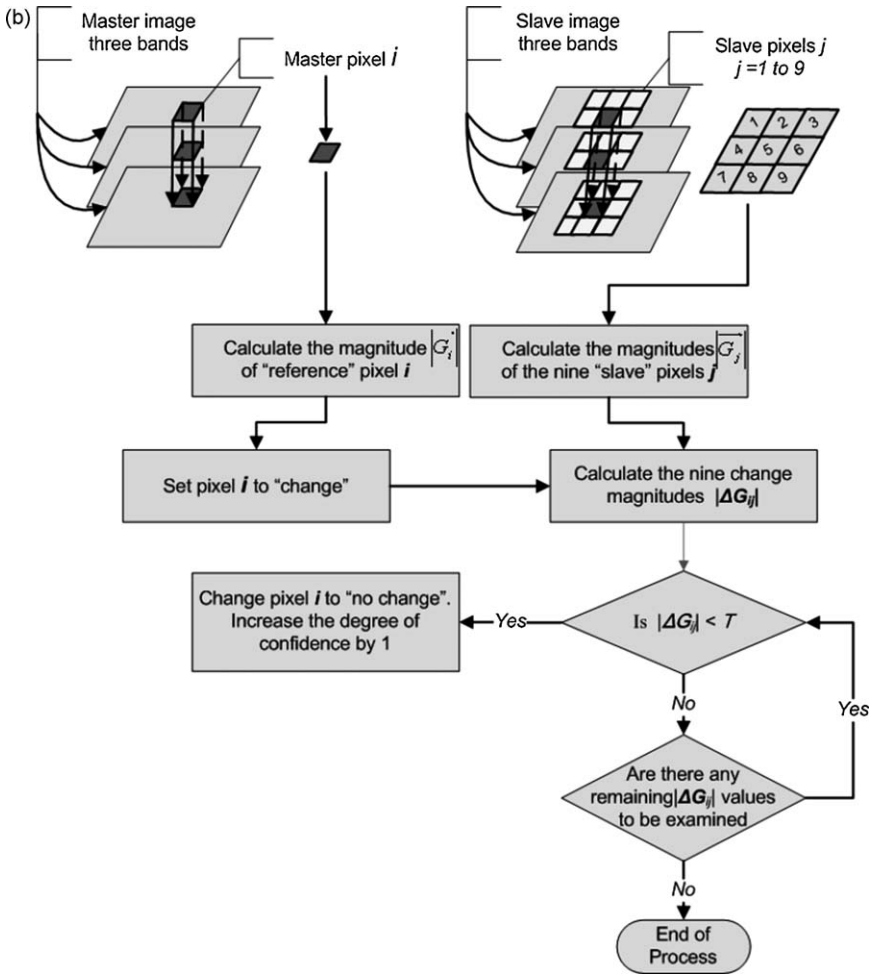

Fig. 3. (*Continued*).

(i) Convert the raster ROI maps to vector polygons and smooth the resulted shapes in order to reduce the "pixel" effects along the polygon borders.
(j) Generate the final BSM shape files in GIS format.

3.2.2. Biophysical processing

The so-called "biophysical processing" aims to produce layers of absolute physical information using the spectral data recorded at pixel level. It is based on the knowledge of optical properties of nature main contributors such as soil, vegetation foliage, water, and the use of radiative transfer models to simulate the signal measured at sensor level. As mentioned, the Overland tool is used for biophysical processing and biophysical layer generation, incorporating state-of-the-art reflectance models, namely:

- The SAIL-PROSPECT model for vegetation. SAIL (Verhoef, 1984 and Verhoef, 1985) is a radiative transfer model that has been extensively validated and it was selected among several other models (Jacquemoud et al., 2000). PROSPECT (Jacquemoud and Baret, 1990) is a reference in terms of modelling the leaf optical properties.
- A proprietary semi-physical model for soil mapping with the capability to capture spectral profiles of soils at local scale.
- The LOWTRAN/MODTRAN model for modelling the atmospheric transmission (Kniezys et al., 1996).

Overland performs autonomous atmospheric correction (i.e. no use of external information on atmospheric conditions) through inversion of a coupled scene/atmosphere model, in a scheme similar to the one presented by Verhoef and Bach (2003). Subsequently, the Overland biophysical processing (Fig. 4) generates a number of information layers as follows:

- Firstly, the algorithm generates layers describing the composition of each pixel in terms of percentage (%) of vegetation cover–green and brown–soil and water, if present on the image plane.
- As long as any of these contributors to the pixel's composition (soil, vegetation, water) is considered significant, the program produces additional information layers characterising it. That is, for vegetation parameter the "canopy shadow factor" is produced characterising the canopy roughness. Similarly for soil parameter the "soil brightness" information is generated, and so on.

Within the BSM_ITF processing chain, Overland is used quite straightforwardly in order to produce:

- Vegetation information layers to discriminate between different land cover types (e.g. forests versus shrubs or crops) and vegetation density classes.
- Soil information layers to simply characterise bare soils and burnt area soils.
- Water and cloud information layers.

3.2.3. Decision tree classification

A decision tree classifier is a set of hierarchical rules, which are successively applied to the input layers. These rules are thresholds which are used to split the data into two groups (binary splits).

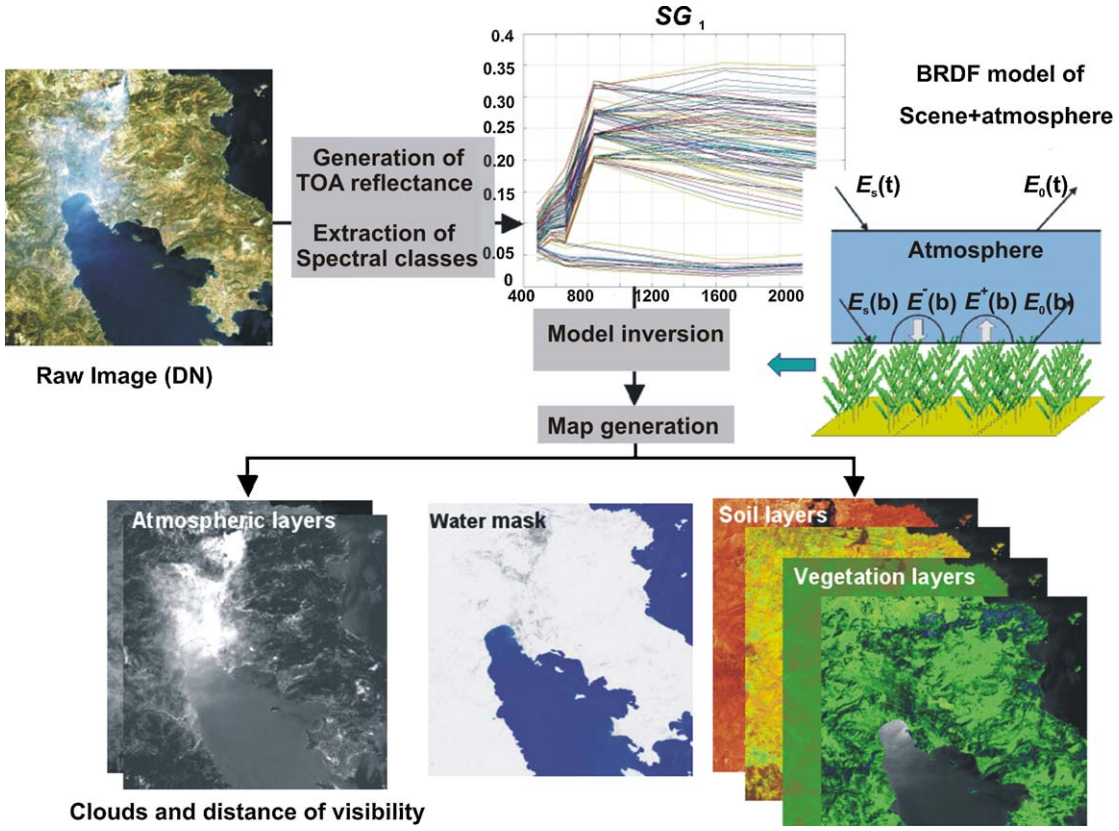

Fig. 4. Illustration of the Overland biophysical processing.

Each split (also called node) is such that the descendant nodes contain more homogeneous data samples (purer in terms of classes). Decision tree classifiers have been successfully applied to remote sensing data in the past (Fries et al., 1998; Hansen et al., 1996; Simard et al., 2000). The decision tree approaches do not rely on any a priori statistical assumption, and due to this they may be suitable for classifying any type of image data. Moreover, the decision tree rules are explicit and allow for identification of features, appropriate to distinguish specific classes, thus limiting the analysis to the most useful information layers. Finally, the structure of the decision tree can also reveal hierarchical and nonlinear relationships among input layers. These relationships often result in a given class being described by terminal nodes (Simard et al., 2000).

In the case of the BSM_ITF application, simple rules can be defined using the biophysical layers generated by Overland and they rely on a limited number of layers that are listed as in Table 1.

The software suite includes an integrated decision tree classifier exploiting the biophysical layers (Fig. 5). It is a user-friendly tool (Fig. 6) enabling the analyst to interactively build the decision tree and adjust threshold values used in the tree with real-time visual validation of the results. The rules for the decision may differ depending on whether it is a uni- or multi-temporal analysis:

- If pre- and post-fire image acquisitions are available, the classification uses parallel indication, especially where dense pre-existing vegetation with rough canopy type (forest or scrubland) did disappear, and that the same area in the post-fire image is dark bare soil (sign of fire ashes). This change is a robust evidence of burnt areas.
- If a single post-fire image is available, identification of burnt areas relies on the dark bare areas (no vegetation) without having any knowledge of the type of vegetation existing before the fire.

Table 1
Biophysical layers routinely used for BSM application.

Name	ID	Description
Green cover fraction	*glcv*	% of pixel covered by green vegetation
Canopy shadow factor	*csh*	% of surface shadows on the vegetation canopy (from 0 – flat canopy – to 100% – very rough canopy – cast shadows)
Soil cover fraction	*scv*	% of soil visible in the pixel
Soil brightness	*sb*	Soil reflectance mean brightness in the visible domain
Water fraction	*wcv*	% of water visible in the pixel
Cloud reflectance	*dcl*	Apparent reflectance of the cloud layer

3.2.4. Generation of final burn scar maps

The next steps are intended to produce a final map of burn scars, having filtered noisy pixels and processed each fire area to the maximum extension of the fire. To achieve this, all pixels initially marked as burnt vegetation are considered as "fire seeds". A 5×5 sliding window is used to compute fire seeds density and to keep fire seeds only above a given density threshold. Subsequently, another buffer window of 15×15 is used to collect and aggregate all burnt vegetation within the corresponding distance of "certified" fire seeds, in order to identify individual fire areas and to produce a Region Of Interest (ROI) for a given fire area. Finally a region growing process is employed that uses the post-fire green cover map (biophysical layer generated by Overland) to make the ROI of each individual fire to grow to the maximum extension of the area without any green vegetation (assuming that the fire did propagate through the whole area). The operator visually inspects the output of this process and the parameterisation of the region growing process is adjusted accordingly, if

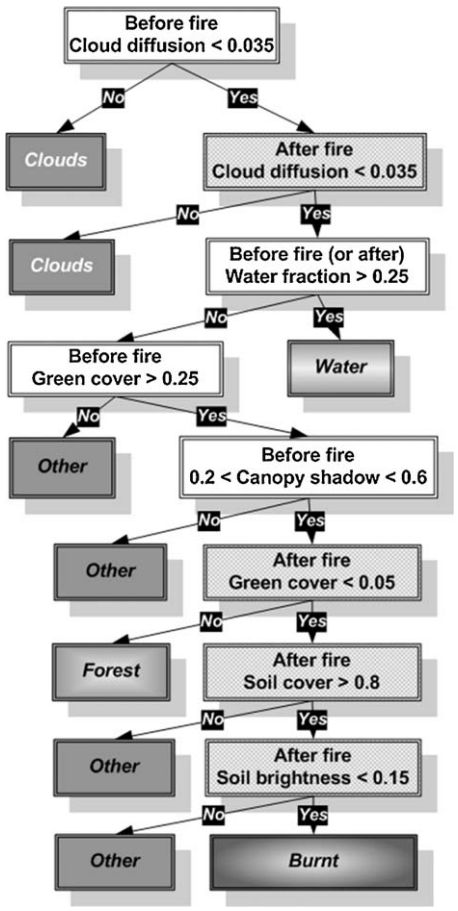

Fig. 5. Typical BSM_ITF decision tree modelling using two date acquisitions (pre- and after-fire images).

necessary. Finally, the raster result is converted to vector BSM polygons. At this stage a quality check is performed and any manual adjustments are made where necessary (e.g. hole filling). Ultimately a line-smoothing algorithm allows reducing the "pixel" effects along the boundaries and the resulted lines are "closed and cleaned" to generate BSM polygons in standard GIS format. Fig. 7 in the following illustrates the successive steps of BSM_ITF processing chain.

3.3. Validation of performance

Since the two methods are standardised RISK-EOS services, their validation is based on a specific validation plan, which clearly identifies the service management, service delivery, user's interaction, data processing chain, and the models and algorithms used. It is a key quality control mechanism approved by ESA that guaranties the integrity and appropriate accuracy of the delivered products.

In this framework the accuracy level of the two methods, BSM_NOA and BSM_ITF, was assessed using an independent reference dataset provided by the regional Forestry Services. The reference data were analogue maps depicting the damaged areas in the scale of 1:50.000. They were generated through dedicated in-situ field campaigns. To enable overlay and facilitate the comparison with the BSM_NOA and BSM_ITF generated burnt area polygons, these maps were transformed to vector GIS products. Moreover, the reference dataset was complemented with information extracted from existing fire logs, reporting the fire occurrence date, duration and location, the size of the affected areas, the names of the affected communities, the types of the damaged forest species, and the means employed for fire suppression.

The surface accuracy figures were expressed in terms of detected area efficiency, skipped area rate (omission error) and false area rate (commission error). These accuracy figures were calculated on the basis of the following formulae:

$$Detected\ Area\ Ef\ ficiency = \frac{DBA}{DBA + SBA}, \tag{5}$$

$$Commission\ Error\ (Flase\ Area\ Rate) = \frac{FBA}{DBA + FBA}, \tag{6}$$

$$Ommission\ Error\ (Skipped\ Area\ Rate) = \frac{SBA}{DBA + SBA}, \tag{7}$$

where *DBA* is the Detected Burnt Area (common area between the generated burn scar polygon and the reference in-situ polygon), *FBA* is the False Burnt Area (area included in the generated burn scar polygon but not in the reference in-situ polygon) and *SBA* is the Skipped Burnt Area (area included in the reference in-situ polygon but not in the generated burn scar polygon).

In addition to surface accuracy assessments, the comparison of the number of fire events detected by each BSM method against to the number of events reported in the available fire logs was also taken into consideration, as an additional measure of the success of each method.

4. Results

The two methods were exhaustively carried out in a comparative manner in three important fires in Greece and these are described in the following paragraphs.

4.1. 2006 Fire season: Using a multi-temporal set of Landsat 5 TM images over Peloponnesus, Greece

4.1.1. Background

In 2006 the number of forest fires in Greece was comparable to the events of previous years and the total burnt area remained lower than the annual mean of the last decade as stated in Report No. 7: Forest Fires in Europe, 2006, issued by The Institute for Environment and Sustainability of the Joint Research Centre. However, the extreme weather conditions during the second half of August and the first days of September facilitated the outburst of major destructive wildfires in the Region of Central Macedonia (prefecture of Chalkidiki–Kassandra peninsula) and the Region of Peloponnesus (prefecture of Lakonia–municipality of Mani). The fire in Mani municipality was burning for four days, with a fire front extending from the cities of Gythio to Areopolis (Fig. 8a). Despite optimism in the first days that the fire of Mani would soon be brought under control, an increase in wind velocity hampered the fire-fighting effort. Propagating quickly and exposed to strong winds the flames destroyed 3750 ha of land including wild land to urban interface areas in which numerous houses and agricultural operations like bee–keepers, and cultivations were previously situated. More than 220 fire fighters backed by fire engines, fire-fighting planes and helicopters, were battling the blaze but at the end the fire burned homes, farm cultivations and forest expanses. At the same time, other fires co-occurred in the forested areas of Chrysovitsi in Arcadia prefecture and at the top of Mt. Mainalos (Fig. 8a) also in the region of Peloponnesus, which were contained by land forces.

4.1.2. BSM processing

Burn scar mapping in the region of Peloponnesus was based on a multi-temporal set of images consisting of four Landsat 5 TM

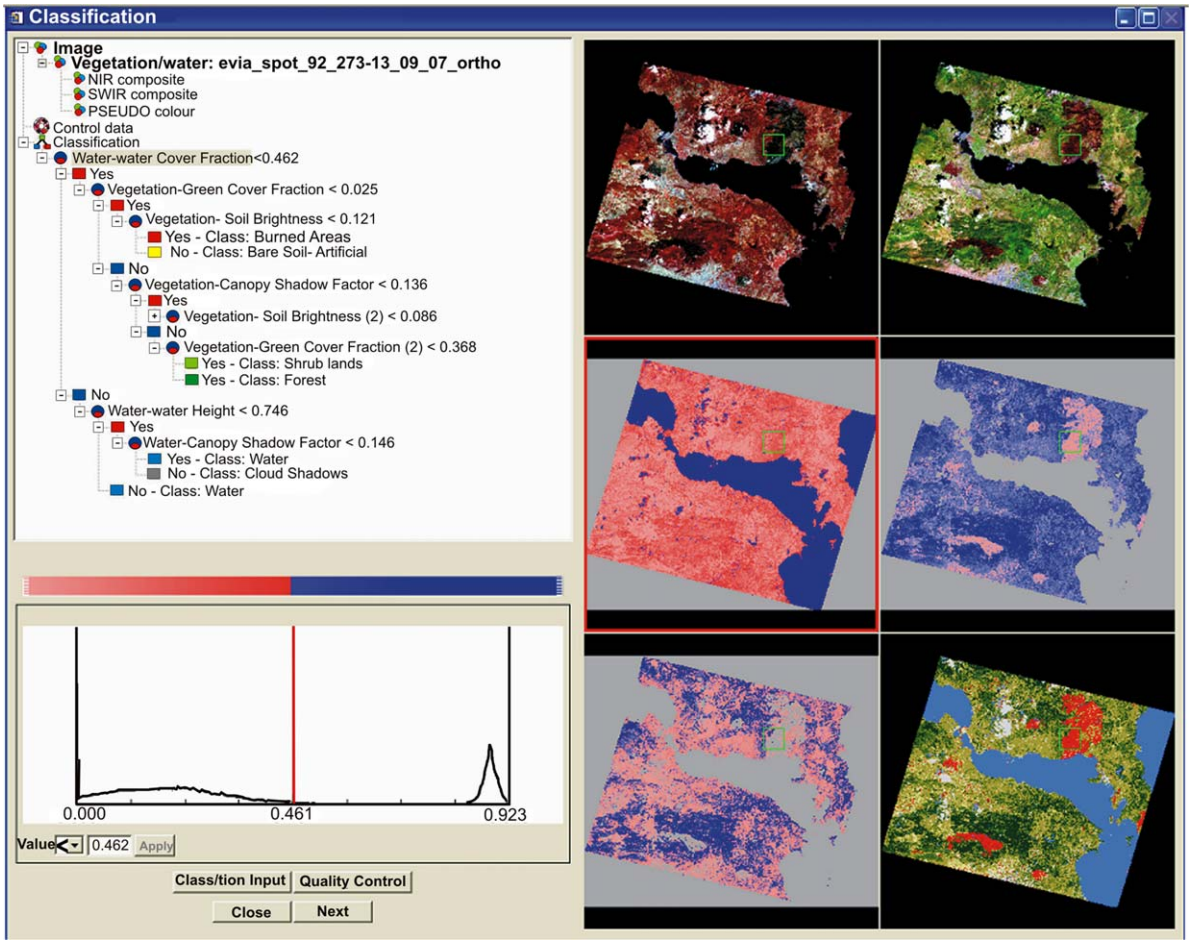

Fig. 6. The Overland interactive window developed to facilitate the user interaction.

acquisitions (path/row: 183/034 and 183/035 acquired on 29-05-2006 and 04-10-2006), covering a total surface of 18,350 km^2 (Fig. 8b). The TM images were ortho-rectified at sub-pixel level using detailed reference topographic maps (1:5000), and the SRTM (Shuttle Radar Topography Mission) digital elevation model. Cloud, shadow and water masking were based on a single image thresholding approach. Cloud masks were initially created by thresholding Landsat TM band 1. Measurements were also taken representing the cloud-to-ground image displacement due to sun angle. Then, an automated process selected all pixels in the image complying with the cloud threshold values. The selected pixels were buffered by three pixels and then projected using the cloud-to-shadow displacement vector. Moreover, thresholding Landsat TM bands 4 and 5 resulted in creating masks of water and shadowed surfaces. All raster layers were then combined to one mask, which was used to remove cloud, shadow and water pixels from the images. Finally, photo-interpretation of the results and manual editing, wherever the latter was necessary, allowed removing any remaining classification errors. In general this process slightly overestimated the cloud, shadow and water areas to ensure that the remaining pixels were free from their influence.

Following pre-processing the two BSM methods were applied. Fig. 9 illustrates the burn scar areas generated by the BSM_NOA and BSM_ITF methods in the Mani municipality. The surface accuracy assessments, referred to as detected area efficiency rate, skipped area rate and false area rate, were calculated using Equations 5, 6, and 7.

The omission error, expressed as the rate of skipped burnt areas, was estimated to be of 23% for BSM_NOA (Table 2) and 21% for BSM_ITF (Table 3) methods respectively. However, it should be noted here that several of the omission errors detected, did not correspond to real examples of skipped surfaces. In reality they were corresponding to 'islands areas', not affected by the fire, located inside greater burned area polygons (the so-called 'donut' polygons). These polygons were correctly attributed by the two BSM approaches to non-burnt surfaces. However, the fact that these surfaces were not appearing on the reference maps, resulted in a number of false cases of omission error (Fig. 10).

Table 2
BSM_NOA method accuracy achieved by using a multi-date set of four Landsat 5 TM images over the region of Peloponnesus; two of the scenes were acquired before and the other two after the fire occurrence.

Accuracy_code	Detected burnt areas	False burnt areas	Skipped burnt areas	Statistics (%)	
2006 Fire Season: Results of BSM_NOA method using multi-date Landsat 5 TM images					
Detected burnt areas (ha)	6254.768			Detection efficiency rate	0.77
False burnt areas (ha)		373.8251		Commission error (False alarm rate)	0.06
Skipped burnt areas (ha)			1904.7120	Omission error	0.23

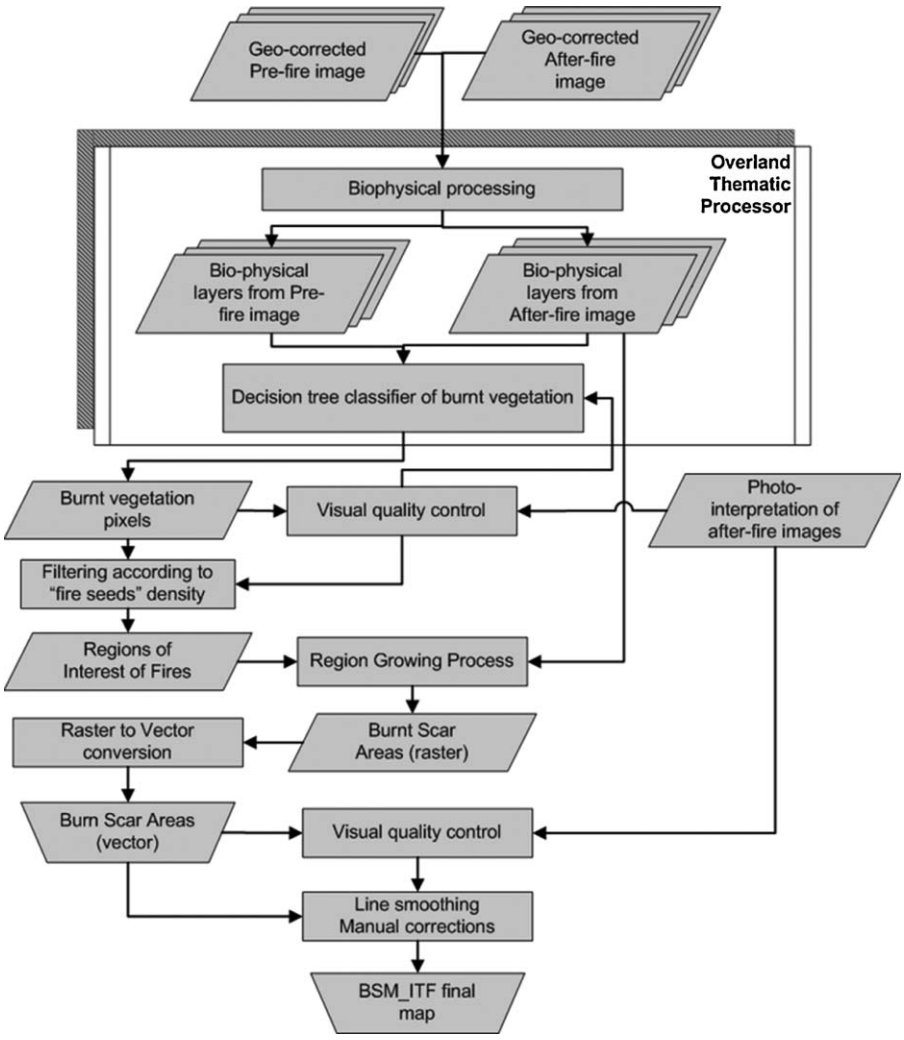

Fig. 7. Flow diagram of the BSM_ITF multi-temporal processing chain.

On the other hand the commission errors (false alarm area rates) were estimated by Equation 6 to be of the order of 6% and 14% for BSM_NOA and BSM_ITF methods, respectively. It is worth noting here that several of these omission error cases were not referring to forests but to olive tree parcels and other permanent crop cultivations spread inside the forested zones. As these parcels were corresponding to unique registrations in the olive and vineyard cadastral systems used in Greece, they were identified and delineated on the reference maps used. However, the same parcels were not possible to be identified by any of the two BSM methods, since the spectral characteristics of olive trees and forest classes were very similar on the pre- and post-fire image acquisitions. With the exception of this type of confusion referring to dense olive cultivations, the two BSM methods identified and separated correctly all parcels of yearly crops, open fields, bare soils and harvested fields located inside the forested zones due to their distinct spectral appearance compared to burn surfaces.

In general, the rates of omission and commission errors (Tables 2 and 3) returned, were remarkably lower than the tolerance limit of 35% defined by the RISK-EOS validation protocol. It is also stressed that they express rather deviations from the reference validation polygons used than the reality. Another interesting outcome relates to the fact that the minimum size of fires detected by the two methods using Landsat 5 TM data, was of 0.9–1.0 ha.

The number of fire events detected by the BSM methods compared to the number reported in the available fire logs was also considered as a measure of success of each method. According to this measure the detection capability for BSM_NOA and BSM_ITF methods, has been estimated to be of 88% and 85% respectively. In practice the BSM_NOA method did not detect

Table 3
BSM_ITF method accuracy achieved by using a multi-date set of four Landsat 5 TM images over the region of Peloponnesus; two of the scenes were acquired before and the other two after the fire occurrence.

Accuracy_code	Detected burnt areas	False burnt areas	Skipped burnt areas	Statistics (%)	
2006 Fire Season: Results of BSM_ITF method using multi-date Landsat 5 TM images					
Detected burnt areas (ha)	6731.7864			Detection Efficiency Rate	0.79
False burnt areas (ha)		1141.6116		Commission Error (False Alarm Rate)	0.14
Skipped burnt areas (ha)			1767.8444	Omission Error	0.21

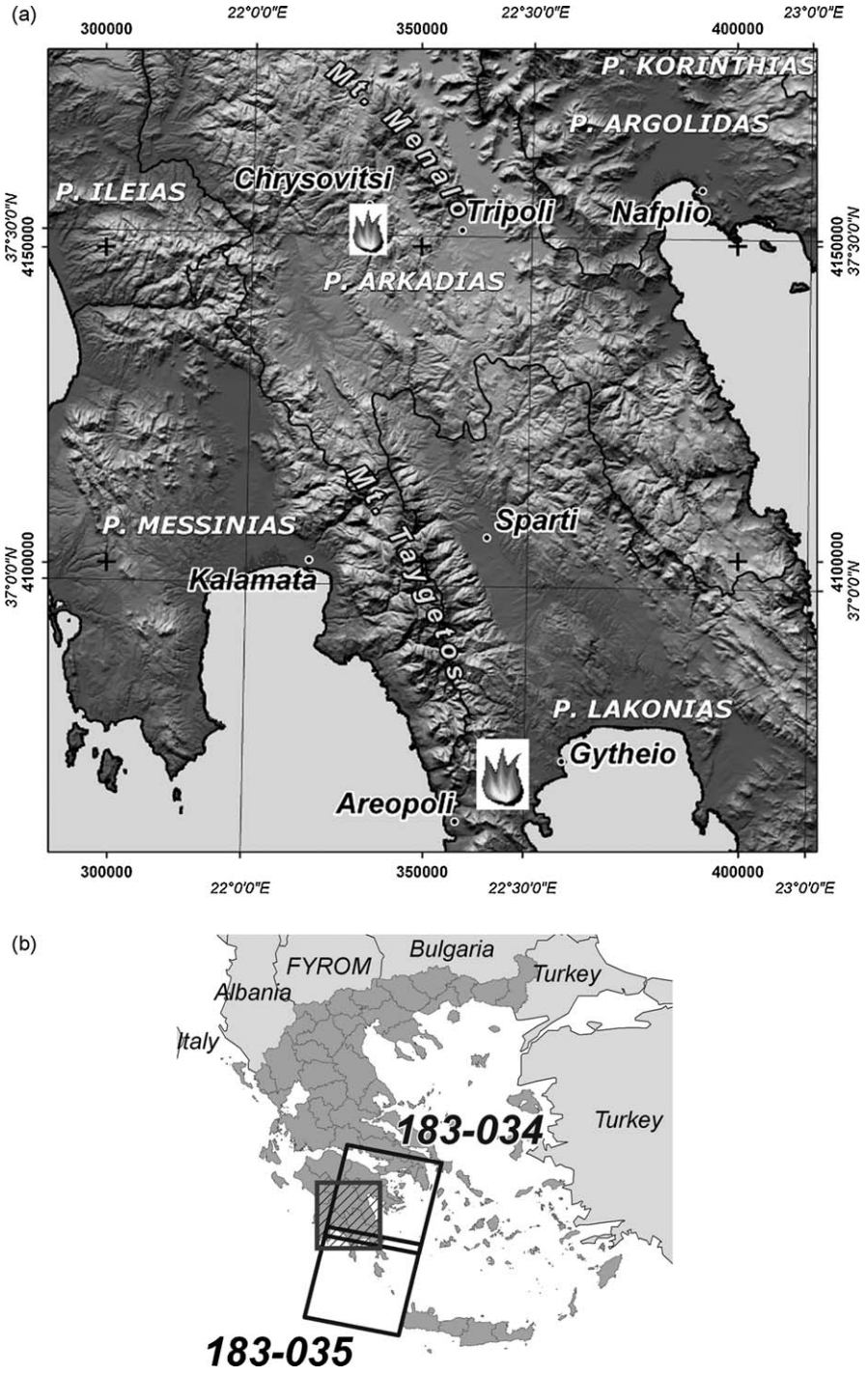

Fig. 8. (a) The location of the Mani fire in the region of Peloponnesus, (b) The area covered by the two Landsat TM frames 183/034 and 183/035.

four out of the thirty-three (4/33) fire events reported in the fire logs and correspondingly the BSM_ITF method missed six fire events out of the thirty-three (6/33) ones reported. It is worth noting that four (4) of the missing fires were common for both methods and their size ranged from 0.8–2.5 ha (small events). Another common characteristic was that they were all located at high altitudes, at steep and washed out terrains, sparsely covered with low biomass bushy and herbaceous vegetation or pasture-lands. Because of this, the strong reflectance of soils hindered the detection of burnt surface. None of the calculated image enhancements including NBR, Albedo, NDVI, soil brightness, and green cover showed any notable difference in the pre- and post-fire acquisitions. As a general conclusion it can be stated that the two methods showed a rather similar detection capability throughout Greece.

4.2. 2007 Fire season: Using a single-date Landsat 5 TM image acquisition over Athens and Peloponnesus, Greece

4.2.1. Background

The 2007 fire season was marked by a series of massive forest fires that broke out in several areas across Greece. Some of these firestorms are believed to be the result of arson whilst others were indeed the result of mere negligence. Hot temperatures that were experienced during three consecutive heat waves of over 40 °C, and severe drought rendered the 2007 summer unprecedented in

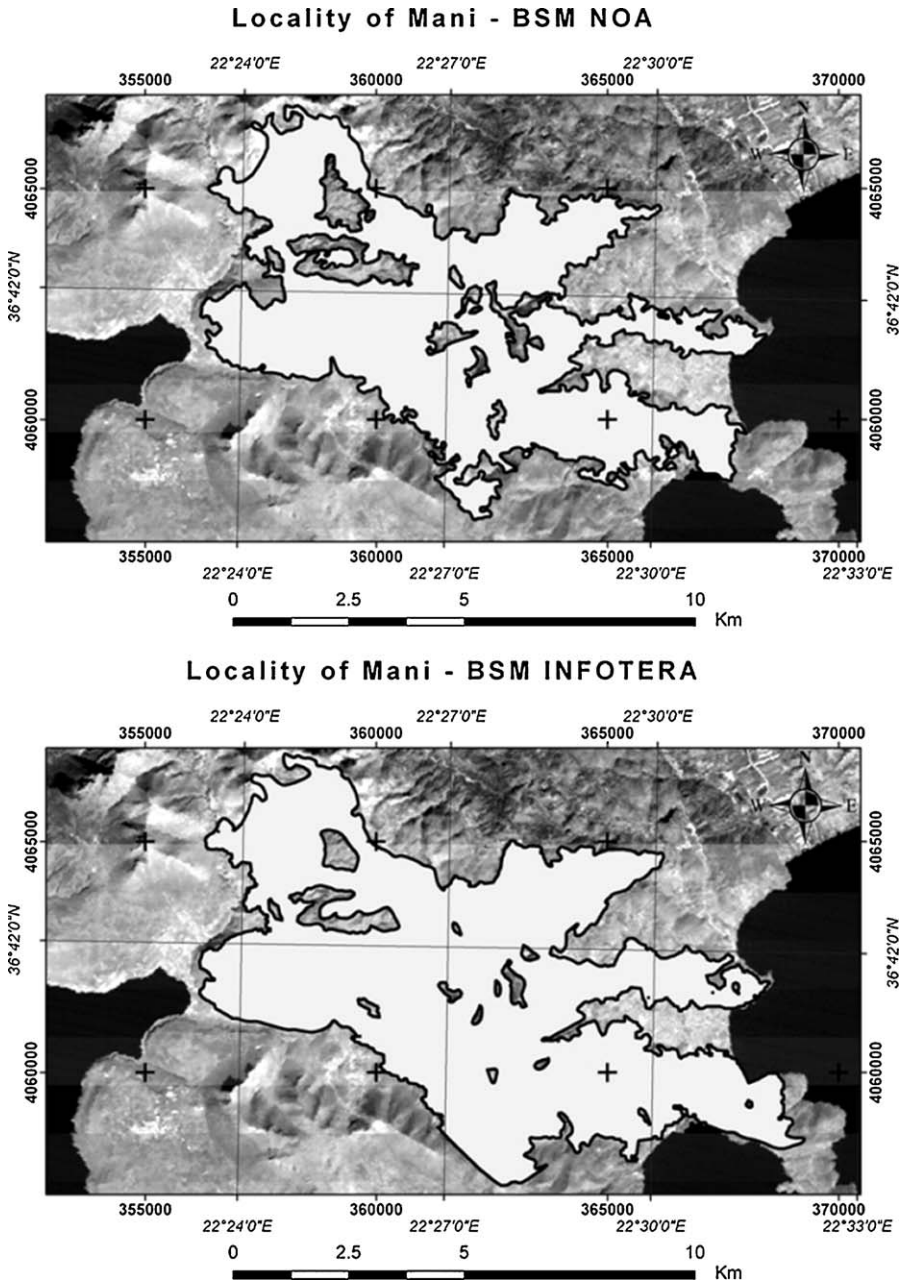

Fig. 9. Burn Scar Mapping in the locality of Mani generated by the BSM_NOA (top frame) and BSM_ITF (bottom frame) methods.

Greek history. From the end of June to early September, hundreds of forest fires were recorded across the country. According to the BSM_NOA mapping estimations over entire Greece, a total of 193656.39 ha of forest, olive groves and farmlands were destroyed in the fires, which was the worst fire season on record in the past 50 years. About sixty per cent of the total surfaces affected were forests located in Southern Greece alone. The fires killed 84 people including fire fighters. Fires trapped many villages, and hundreds of houses and buildings were destroyed in the blaze.

The first major fire of that season occurred on June 28, 2007 on the top of Mt. Parnitha to the north of the city of Athens (Fig. 11). It is perceived to have started by either an exploding electrical pylon or by arsonists. The magnitude of the devastation was unforeseen. The fire consumed forests in two prefectures. Fire fighters, helicopters, and planes were brought into action across the mountain area and its edges fighting the enormous blaze, which took days to contain. Significant parts of the Parnitha National Park were destroyed, and in total, this fire burnt 4726 ha of the core of the national forest in a few days, making it one of the worst recorded wildfires in Attica. The fire claimed an 80% proportion of the *rare Greek Fir and Aleppo Pine* forest, and many animals of the red deer population (an endangered species), birds, and other rare species. Scientists estimate that the *Greek Fir* recovery time may be as long as a century, as it is a mountainous species not adapted to fires.

4.2.2. BSM processing

Immediately after the fire was contained, the authorities requested precise maps from the affected area. In order to respond to this prompt demand it was decided to use the first single-date Landsat 5 TM post-fire image acquisition, which became available on July 19, 2007 (path/row: 183/034). The image underwent all necessary processing steps including radiometric calibration and ortho-rectification, as well as BSM_NOA and BSM_ITF processing and post-processing. In this specific case, the BSM_NOA approach was based on the thresholding of a single-date NDVI image [Eq. (2)] instead a multi-date one. The same approach has been used in

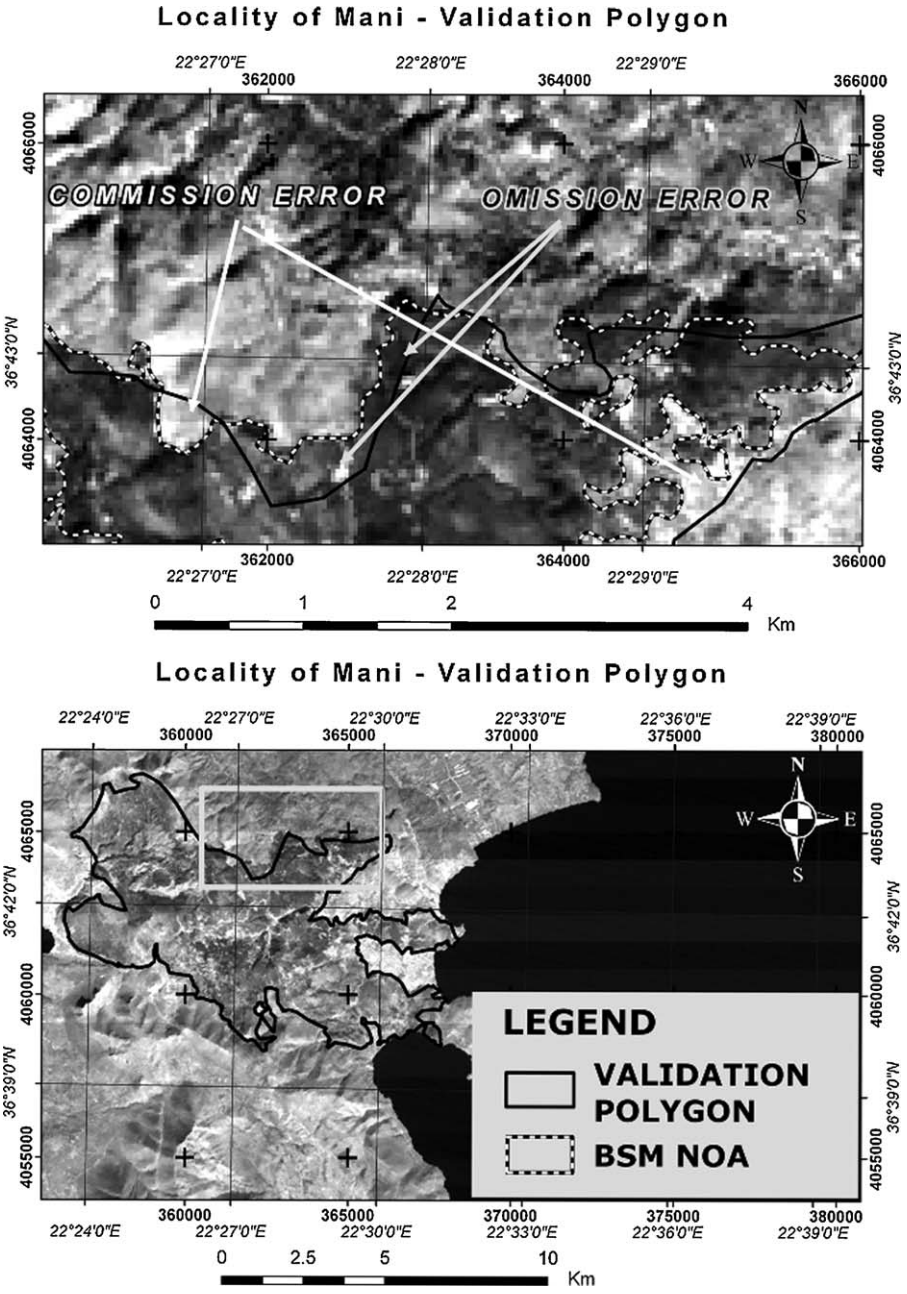

Fig. 10. Errors of omission and commission imported in the validation process due to lower quality reference data used (top frame). Polygon used for the validation of the Mani fire event (bottom frame).

several single-date fire mapping studies in the past (Diaz-Delgado and Pons, 2001; Vafeidis and Drake, 2005; Li et al., 2000).

At that time no reference data were available for validation. According to the usual practice the regional forestry departments initiate the burn scar mapping operations at the end of the fire season. For this and in order to generate a reliable set of validation data throughout the affected area, specific GPS measurement campaigns and post-fire aerial photography interpretations were undertaken by ISARS/NOA.

Overall, BSM_NOA showed higher sensibility in identifying small size burn scars (approximately 0.5–2.0 ha). Comparing the outcome of the two methods with the existing fire records, it was inferred that only four small events, summing up to a total surface of 14.35 ha, were not mapped by the BSM_ITF method. This error accounts only for the 0.2% of the total burnt surface detected on the Landsat 5 TM image processed. As for the BSM_NOA method, it should be noted that there were not reported any cases of omitted fires compared to existing fire logs. This can be explained as in the following. Since the entire process was based on single-date data, there remained several mapping uncertainties corresponding mainly to small size and less intensive fire events. These uncertainties could not be resolved than using human interpretation. It is then believed that at this stage, the team of French interpreters who dealt with the deployment of the BSM_ITF method in Greece were not able to resolve every case of uncertainty, due to their limited experience in the interpretation of the complex and highly fragmented landscape environment of Greece.

Based on the adopted validation protocol the overall efficiency of BSM_NOA and BSM_ITF methods for burnt area detection (Tables 4 and 5) were estimated to be as high as 87% and 82% respectively, with the omission ('skipped areas') errors being 13% and 18% and commission (false alarms) errors as low as 3% and 5%, respectively. The 'skipped areas' corresponded to cases of surface fires burning the under tree cover without reaching the crown top.

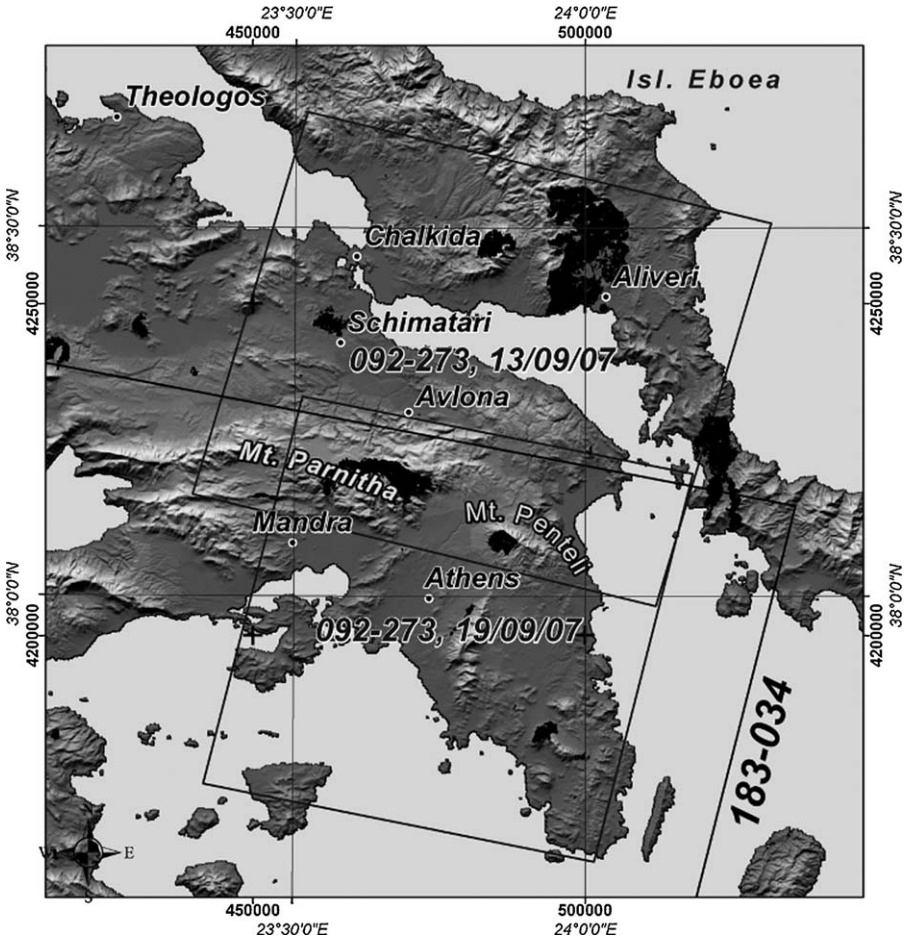

Fig. 11. The location of Parnitha and Penteli fires in Attica and the location of the Aliveri fire in Euboea Island. The SPOT XS and Landsat TM frame coverage is also illustrated.

Due to this the treetops have remained partly or totally unaffected reflecting back to the satellite sensor as healthy vegetation. Fig. 12 illustrates the Parnitha fire extent mapped by the BSM_NOA and BSM_ITF methods as well the omission and commission errors reported in respect to reference validation data used.

4.3. 2007 Fire season: Using a single-date SPOT 4 XS image acquisition over Euboea and Athens, Greece

4.3.1. Background

The Parnitha National Park catastrophe was followed by new fires, which started to burn the outskirts of Athens on August 17, 2007, at Penteli Mt. and continued burning down towards the suburbs of Athens (Fig. 13). The Athens municipalities of Melisia, Vrilisia and Penteli were affected by the blaze that was put out only after the strong winds subsided. In addition, large devastating fires broke out in Euboea island at the vicinity of Eretria and Stira municipalities on August 24, 2007. Euboea island (Fig. 13b) was struck by the worst fires ever reported in its history. The fires spread very quickly to the north passing through the surroundings of the city of Aliveri on August 25, 2007 and then turning to the north not far from the Dirfys mountain ranges consuming hundreds of hectares of dense pine and spruce forests in a few hours. Moreover, many hotels, restaurants and tourist infrastruc-

Table 4
BSM_NOA method accuracy achieved using a single-date Landsat 5 TM image over Parnitha National Park.

Accuracy_code	Detected burnt areas	False burnt areas	Skipped burnt areas	Statistics (%)	
2007 Fire Season: BSM_NOA accuracy results, Parnitha National Park					
Detected burnt areas (ha)	4593.79			Detection efficiency rate	0.87
False burnt areas (ha)		132.11		Commission error (false alarm rate)	0.03
Skipped burnt areas (ha)			699.74	Omission error	0.13

Table 5
BSM_ITF method accuracy achieved using a single-date Landsat 5 TM image over Parnitha National Park.

Accuracy_code	Detected burnt areas	False burnt areas	Skipped burnt areas	Statistics (%)	
2007 Fire Season: BSM_ITF accuracy results, Parnitha National Park					
Detected burnt areas (ha)	4491.60			Detection efficiency rate	0.82
False burnt areas (ha)		253.58		Commission error (false alarm rate)	0.05
Skipped burnt areas (ha)			1001.93	Omission error	0.18

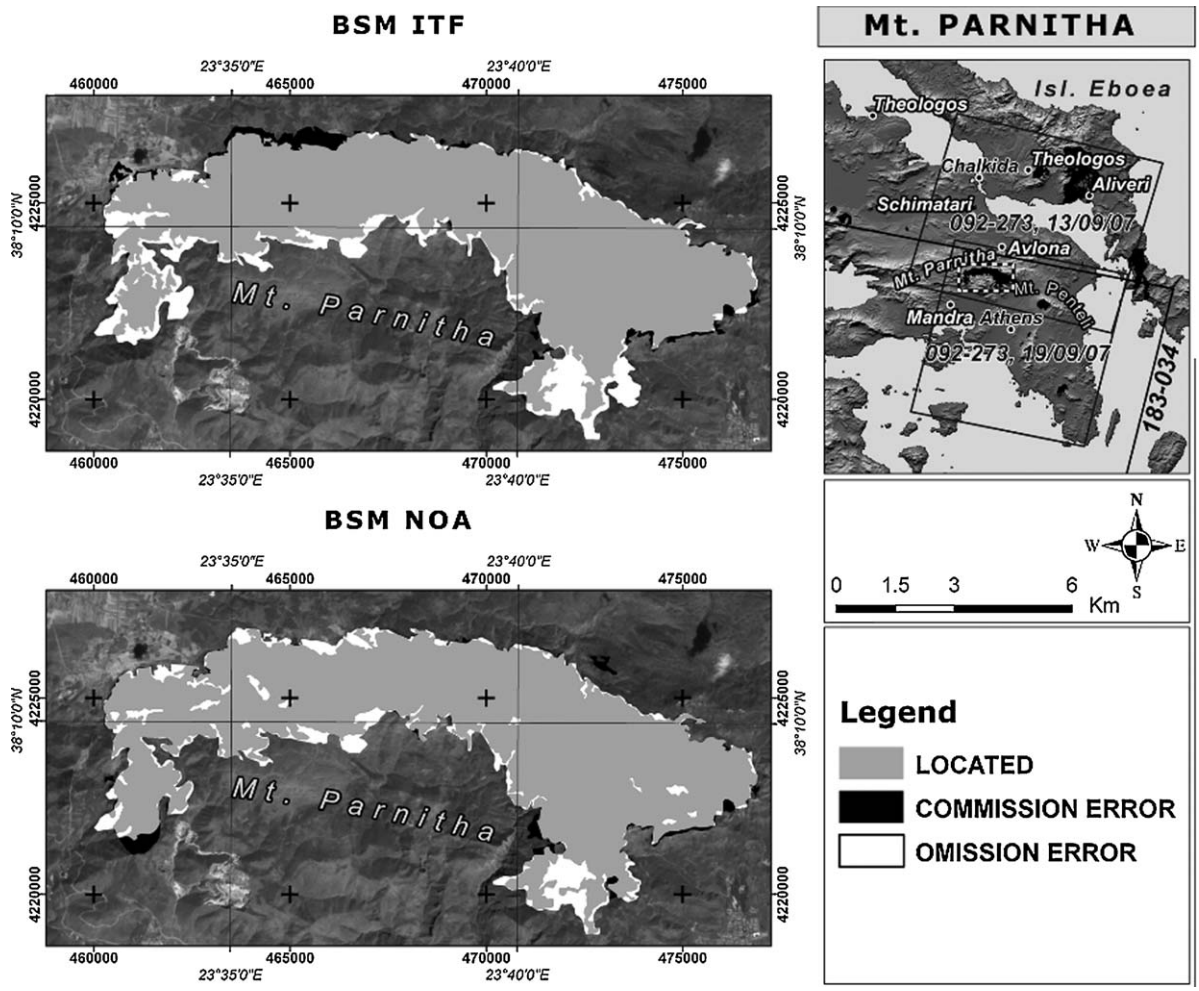

Fig. 12. Burn Scar Mapping in the case of Parnitha fire using BSM_ITF (top left) and BSM_NOA (bottom left) methods. Cases of omission and commission errors in respect to the reference validation data used are obvious.

tures were destroyed. Fire fighters battled the blaze along with helicopters and planes, several of them coming from international assistance.

4.3.2. BSM processing

These fire events were mapped using a single-date SPOT 4 XS image that was acquired early after the fire season on September 29, 2007 (path/row: 092/272). This acquisition depicted the Euboea-Aliveri fire as well as the ones of Parnitha Mt., and Penteli Mt. and a number of other smaller fires in the surroundings. The image underwent all necessary pre-processing steps including radiometric calibration and ortho-rectification. The BSM_NOA and BSM_ITF approaches were applied on the single-date SPOT XS image acquisition in order to assess the fire damages in the affected regions.

The two methods performed similarly to the single-date Landsat 5 TM image acquisition as far as the detection capability and surface accuracy figures were concerned. Twelve fire events were identified by BSM_NOA on the SPOT 4 XS image, the larger ones being those of Aliveri (13,235 ha), Parnitha (4726 ha), Penteli (902 ha), Theologos (1362 ha), Schimatari (939 ha), Mandra (185 ha), and Avlona (4 ha). Five more, however much smaller, fires of the size of 1–2.5 ha were also identified and mapped. The BSM_ITF method however did not succeed to return four out of the five smaller fires, summing up to a rather negligible surface error of 0.04% compared to the total burnt surface detected over the entire SPOT 4 XS image.

In relevance to Penteli fire, the overall efficiency of BSM_NOA and BSM_ITF methods for burnt area detection were estimated to be as high as 91% and 85% respectively (Tables 6 and 7), with the omission (skipped areas) errors being 9% and 15% and commission (false alarms) errors as low as 6% and 4%, respectively. The results are presented in Tables 6 and 7. Considering now the BSM_NOA results, the majority of the surfaces labelled as 'omitted', did not correspond to real cases of skipping actual fire events. Actually they corresponded to old mines of Mt. Penteli not affected by the

Table 6
BSM_NOA method accuracy achieved using a single-date SPOT XS image acquisition over Penteli Mt.

Accuracy_code	Detected burnt areas	False burnt areas	Skipped burnt areas	Statistics (%)	
2007 Fire Season: BSM_NOA accuracy results using single-date SPOT 4 XS data					
Detected burnt areas (ha)	851.63			Detection efficiency rate	0.91
False burnt areas (ha)		50.30		Commission error (false alarm rate)	0.06
Skipped burnt areas (ha)			83.60	Omission error	0.09

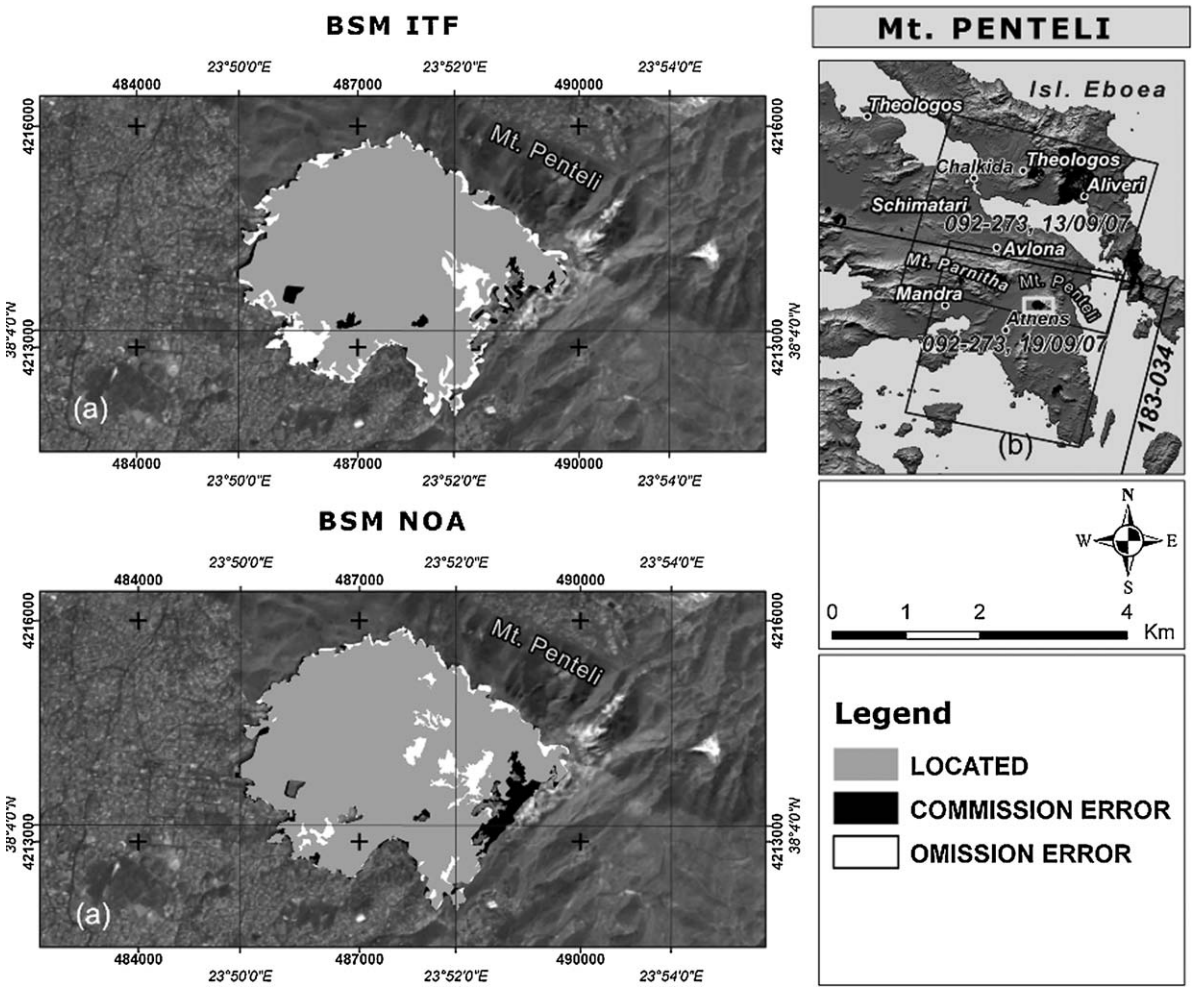

Fig. 13. (a) Burn Scar Mapping in the case of Penteli fire using BSM_ITF (top left) and BSM_NOA (bottom left) methods. Cases of omission and commission errors in respect to reference validation data used are obvious. (b) The locations of Penteli Mt to the northeast of Athens and of the Euboea island are illustrated.

Table 7
BSM_ITF method accuracy achieved using a single-date SPOT XS image acquisition over Penteli Mt.

Accuracy_code	Detected burnt areas	False burnt areas	Skipped burnt areas	Statistics (%)	
2007 Fire Season: BSM_ITF accuracy results using single-date SPOT 4 XS data					
Detected burnt areas (ha)	795.00			Detection efficiency rate	0.85
False burnt areas (ha)		32.68		Commission error (false alarm rate)	0.04
Skipped burnt areas (ha)			135.00	Omission error	0.15

fires. However because they were considered by the Forestry services as subjects of reforestation together with the burnt areas, they were appearing on the reference maps used for validation.

Moreover, the omission errors attributed to BSM_ITF method corresponded to areas located at the fringe of the urban zones in the vicinity of the forested burnt areas. In this particular case it is likely that artificial surfaces and forest tree spectra mixtures had not been accounted properly in the rules used by the decision-tree approach applied by BSM_ITF. Fig. 13 illustrates the Penteli Mt. fire extent mapped by the BSM_NOA and BSM_ITF methods as well the omission and commission errors reported with respect to reference validation data used.

5. Discussion

The two methods are applicable to images with different spectral and spatial resolutions, and can exploit effectively data from different acquisition modes (uni-temporal and multi-temporal). In a multi-temporal approach using a pair of Landsat 5 TM images, both methods performed better than using a single-date image in identifying the post-fire decrease of vegetation vigour and minimizing the spectral confusion of burnt areas with classes such as permanent crops, bare soil, shadows, urban fabric and water. Both methods showed high potential in burnt area detection, whilst the minimum burnt area size detected was approximately 0.9–1.0 ha despite the coarser pixel spatial resolution of 30m. Moreover, the BSM_NOA method performed better compared to BSM_ITF method in the delineation of small fires of ~0.8–2.5 ha located in the alpine zones of the Greek mountains. Another important feature is the high sensitivity of both methods to separate healthy from burnt vegetation, which resulted in the generation of very detailed thematic maps compared even to field data.

However in many large-scale projects a single-date approach is preferred to a multi-temporal one, as it renders the study more competitive and straightforward. Moreover, the rapid fire mapping actions deployed during crisis (e.g. RISK-EOS/GSE project of ESA –

http://www.risk-eos.com, the International Charter for Space and Major Disasters project of ESA – http://www.disastercharter.org), are based solely on single-date acquisitions, as the damage assessment maps are requested within a few hours after the satellite passing. For this, it was important to conclude that the two methods performed satisfactorily also in a single-date mode. Either using a single Landsat 5 TM or a SPOT 4 HRV post-fire image, the two methods competent with the overall accuracy rates reaching 91% and 85% for BSM_NOA and BSM_ITF, respectively. Furthermore, BSM_NOA performed better in identifying small size burn scars – of the order of 0.5–2.0 ha – compared to BSM_ITF.

Another interesting point is the higher thematic accuracy and geometric precision of the generated burnt scar maps compared to the validation polygons (reference dataset). To be noted that the validation polygons had been generated by the Forestry Services during dedicated field campaigns in the Greek regions hit by fire. Comparing the BSM study results with the validation polygons, it was deduced that the in-situ delineation of the burnt areas tends to be a complicated task throughout Greece, and many resources need to be deployed on the filed for attaining the high level of precision and thematic specificity achieved by the two satellite-based mapping approaches. This is clearly shown in Fig. 10, which depicts a common case of validation data used as reference for assessing the accuracy of the generated burn scar maps of Mani (Peloponnesus). The figure illustrates clearly the inherent to the validation data omission and commission errors imported in the accuracy assessments. From this it can be also deduced that the detection efficiency (77% and 79% for BSM_NOA and BSM_ITF methods, Tables 2 and 3, respectively) would have been significantly higher if it had been calculated using more precise and better quality reference data. However, such reference data and detailed cadastral maps do not exist yet in the studied areas and this further highlights the significance of the proposed satellite-based methods for operational mapping studies.

The use of SPOT 4 HRV data has also emphasised the ability to assess the damaged areas based solely on red and near infrared sensor bands. This important finding can be extended to several sensors currently onboard commercial satellites like IRS, IKONOS-2, FORMOSAT-2, or DMC, which include near infrared and red spectral bands. Moreover, as the family of Landsat satellites has been facing serious technical problems since 2003 and there are many arguments justifying the need to replace such data in order to ensure the continuity of the services relating to satellite burn scar mapping, it is essential that the two BSM methods remain flexible in wavelength selection and satellite data used.

As far as data selection is concerned, a trade-off exists when deciding on the optimal spatial resolution range and sensor spectral characteristics. Whilst sensors with very high spatial resolution (e.g. Quickbird, IKONOS-2, FORMOSAT-2) may provide extremely accurate information on a particular fire event, the amount of data generated in attempting to cover large areas may hamper processing the data. However, there are areas like the region of Peloponnesus in Greece, in which the processing of 144 single-date FORMOSAT-2 image acquisitions (72 panchromatic of 2m pixel resolution and 72 multi-spectral of 8m pixel resolution) was considered mandatory to effectively map the impact of the 2007 summer fires. It is important to report here that this was entirely done by using the BSM_NOA method, demonstrating its flexibility in the processing of very high spatial resolution satellite data using the red and infrared bands only (RISK-EOS-ESA final report for phase 2 – ref: RISKEOS2-3000-SOP-NOA-238-BSM_V1[1].0.doc; European Space Agency, 2008).

6. Conclusions

In this paper we presented, tested and evaluated the performance of two burn-scar mapping methods, namely BSM_NOA and BSM_ITF. Both methods were developed within the framework of the RISK-EOS/GSE-ESA program to meet operational fire mapping requirements of institutional users in south European Mediterranean countries. This research study was undertaken to determine the applicability and suitability of the two methods for this task using difference satellite data used in terms of spectral and spatial resolutions as well as acquisition modes (uni- and multi-temporal). The two methods were deployed using both acquisition modes from two different satellite sensors, namely Landsat 5 TM, and SPOT 4 XS HRV. The effectiveness of the two methods and image enhancements used was assessed with respect to successful identification of burnt and unburned vegetation complexes throughout the Greek landscape environment.

The present study provides concrete evidence that the introduced methods offer advanced burnt area mapping in terms of cost and accuracy, compared to conventional field surveys and/or aerial photo-interpretation. The results presented here as well as the overall experience gained through the RISK-EOS/GSE-ESA project (RISK-EOS-ESA final report for phase 2 – ref: RISKEOS2-3000-SOP-NOA-238-BSM_V1[1].0.doc; European Space Agency, 2008), suggest that the satellite-based mapping methods can replace the conventional methods at an accuracy level far exceeding the existing mapping standards established by the Forestry Services in many Mediterranean countries.

The mapping accuracy of the two methods was assessed in a much challenging environment, namely the accentuated relief and highly diversified ecosystems of the mountainous terrains of Greece. Both methods proved highly sensitive in detecting burnt areas avoiding spectral confusion with other classes such as bare soil, urban fabric, water, and permanent crops. They achieved similar accuracies and class thematic representations, with the BSM_NOA method being slightly more advantageous compared to BSM_ITF, likely because the first was developed initially to account for the specificities of the Greek landscape complexities.

The results undoubtedly advocate the using of the two satellite-based approaches for rapid and standardised damage assessment mapping either at communal, regional or even national level, at scales ranging from 1:50.000 up to 1:10.000 depending on the spatial resolution of the satellite data used (Landsat TM, SPOT XS, FORMOSAT 2, IKONOS, etc.).

The methods proved flexible enough to be applied to any study area since they accommodate an interactive approach for the definition and fine tuning of the spectral thresholds in the case of BSM_NOA, and adaptation of the rules in the case of the BSM_ITF tree decision approach. This explains the efficient deployment of the BSM_ITF approach over Greece even though the method was initially developed to address the needs of the French user community for post-fire management. Moreover, they can be easily reproduced either using the same or refined thresholds and rules at any future date. Among the advantages of the methods are also simplicity and processing speed.

In view of the greatly reduced cost, repeatability, flexibility, standardisation and high accuracy obtained by the BSM_NOA and BSM_ITF approaches compared to conventional methods, this study promotes that satellite data and satellite-based approaches are the most suitable solutions for operational burn scar mapping in the framework of EU and national projects.

Acknowledgements

We are grateful to ESA and ESA officers Mr. Marc Paganini, Mr. Mark Doherty and Mr. Pedro Poiares Baptista for supporting the implementation of the RISK-EOS/GSE project to Greece.

References

Arino, O., Piccolini, I., Siegert, F., Eva, H., Chuvieco, E., Martin, P., Li, Z., Fraser, R.H., Kasischke, E., Roy, D., Pereira, J., Stoppiana, D., 1999. Burn scars mapping methods, forest fire monitoring and mapping: a component of global observation of forest cover. In: Abern, F., Gregoire, J.-M., Justice, C. (Eds.), Report of a Workshop, 3–5 November, Joint Research Centre, Ispra, Italy, pp. 198–223.

Boles, S.H., Verbyla, D.L., 2000. Comparison of three AVHRR-based fire detection algorithms for interior Alaska. Remote Sensing of Environment 72, 1–16.

Cahoon, D., Stocks, B., Levine, J., Cofer, W., Chung, C., 1992. Evaluation of a technique for satellite-derived area estimation of forest fires. Journal of Geophysical Research 97, 3805–3814.

Chuvieco, E., Martin, M.P., Palacios, A., 2002. Assessment of different spectral indices in the red near-infrared spectral domain for burned land discrimination. International Journal of Remote Sensing 23 (16), 5103–5110.

Cocke, A.E., Fule, P.Z., Crouse, J.E., 2005. Comparison of burn severity assessments using Differenced Normalized Burn Ratio and ground data. International Journal of Wildland Fire 14 (2), 189–198.

Collins, J.B., Woodcock, C.E., 1996. An assessment of several linear change detection techniques for mapping forest mortality using multitemporal LandsatTM data. Remote Sensing of Environment 56, 66–77.

Diaz-Delgado, R., Pons, X., 2001. Spatial patterns of forest fires in Catalonia (NE of Spain) along the period 1975–1995: analysis of vegetation recovery after fire. Forest Ecology and Management 147, 67–74.

Elmore, A.J., Mustard, J.F., Manning, S.J., Lobell, D.B., 2000. Quantifying vegetation change in semiarid environments: precision and accuracy of spectral mixture analysis and the normalized difference vegetation index. Remote Sensing of Environment 73, 87–102.

European Commission, 2006. Forest Fires in Europe. Report No. 7. Joint Research Centre, Institute for Environment and Sustainability, EUR 22931 EN, ISSN 1018-5593, Luxembourg, Office for Official Publications of the European Communities, p. 78.

European Space Agency, 2008. RISK-EOS final report for phase 2 – ref: RISKEOS2-3000-SOP-NOA-238-BSM_V1[1].0.doc, edited by: Kontoes C, Sifakis N., Keramitsoglou I., p. 49.

Fisher, R., Vigilante, T., Yates, C., Russel-Smith, J., 2003. Patterns of landscape fire and predicted vegetation response in the North Kimberley region of Western Australia. International Journal of Wildland Fire 12 (3–4), 369–379.

Fraser, R.H., Li, Z., 2002. Estimating fire related parameters in boreal forests using SPOT VEGETATION. Remote Sensing of Environment 82, 95–110.

Fries, R.D., Hansen, M., Townshend, J., Sohlberg, R., 1998. Global land cover classification at 8 km spatial resolution: the use of data derived from landsat imagery in decision tree classifiers. International Journal of Remote Sensing 19 (16), 3141–3168.

Fung, T., Jim, C.Y., 1998. Assessing and modelling hill fire impact in country parks with SPOT HRV images and GIS. Geocarto International 13 (1), 47–58.

Gong, P., Pu, R., Li, Z., Scarborough, J., Clinton, N., Levien, L.M., 2006. An integrated approach to wildland fire mapping of California, USA using NOAA/AVHRR data. Photogrammetric Engineering and Remote Sensing 72 (2), 139–150.

Hansen, M., Dubayah, R., DeFries, R., 1996. Classification trees: an alternative to traditional land cover classifiers. International Journal of Remote Sensing 17 (5), 1075–1081.

Jacquemoud, S., Bacour, C., Poilve, H., Frangi, J.P., 2000. Comparison of four radiative transfer models to simulate plant canopies reflectance—direct and inverse mode. Remote Sensing of Environment 74, 471481.

Jacquemoud, S., Baret, F., 1990. PROSPECT: a model of leaf optical properties spectra. Remote Sensing of Environment 34, 75–91.

Kasischke, E., French, H., 1995. Locating and estimating the areal extent of wildfires in Alaskan Boreal Forest, using Multiple Season AVHRR NDVI Composite Data. Remote Sensing of Environment 51, 263–275.

Kasischke, E., French, H., Harrell, P., Christensen, N., Ustin, S., Barry, D., 1993. Monitoring of wildfires in Boreal forests using large area AVHRR NDVI composite image data. Remote Sensing of Environment 45, 61–71.

Kauth, R., Thomas, G., 1976. The Tasseled Cap—a graphic description of the spectral–temporal development of agricultural crops as seen by Landsat. In: Proceedings of the Symposium on Machine Processing of Remotely Sensed Data, West Lafayette, Purdue University, pp. 41–51.

Key, C., Benson, N.C., 2003. The Normalised Burn Ratio (NBR): a Landsat TM radiometric measure for burn severity. http://www.nrmsc.usgs.gov/research/ndbr.htm.

Kniezys, F.X., Abreu, L.W., Anderson, G.P., Chetwynd, J.H., Shettle, E.P., Berk, A., Bernstein, L.S., Robertson, D.C., Acharya, P., Rothman, L.S., Selby, J.E.A., Gallery, W.O., Clough, S.A., 1996. In: Abreu, L.W., Anderson, G.P. (Eds.), The MODTRAN 2/3 Report and LOWTRAN 7 Model. Phillips Lab., Geophys. Directorate, MA 01731, PL/GPOS, Hanscom AFB, Contract F19628-91-C-0132.

Kontoes, C.C., 2008. Operational land cover change detection using change-vector analysis. International Journal of Remote Sensing 29 (16), 4757–4779, doi:10.1080/01431160801961367.

Koutsias, N., 2000. Burned area mapping using logistic regression modelling of a single post-fire Landsat-5 Thematic Mapper image. International Journal of Remote Sensing 21 (4), 673–687.

Koutsias, N., Karteris, M., 2000. Burned area mapping using logistic regression modeling of a single post-fire Landsat-5 Thematic Mapper image. International Journal of Remote Sensing 21 (4), 673–687.

Lasaponara, R., 2006. Estimating spectral separability of satellite derived parameters for burned areas mapping in the Calabria region by using SPOT-Vegetation data. Ecological Modelling 196 (1–2), 265–270.

Leblon, B., Alexander, M., Chen, J., White, S., 2001. Monitoring fire danger of Northern Boreal Forests with NOAA-AVHRR NDVI Images. International Journal of Remote Sensing 22 (14), 2839–2846.

Li, Z., Kaufman, Y.J., Ichku, C., Fraser, R., Trishchekno, A., Giglio, L., Jin, J., Yu, X., 2001. A review of AVHRR-based active fire detection algorithms: principles, limitations, and recommendations. In: Abern, A., Goldammer, J.G., Justice, C. (Eds.), Global and Regional Vegetation Fire Monitoring from Space: Planning and Coordinated International Effort. SPB Academic Pub, The Hague, The Netherlands, pp. 199–225.

Li, Z., Nadon, S., Cihlar, J., 2000. Satellite-based detection of Canadian Boreal forest fires: development and application of the algorithm. International Journal of Remote Sensing 21 (16), 3057–3069.

Li, Z., Cilar, J., Moreau, L., Huang, F., Lee, B., 1997. Monitoring fire activities in the Boreal ecosystem. Journal of Geophysical Research 102, 29611–29624.

Lyon, G.J., Ding, Y., Lunetta, R.S., Elvidge, C.D., 1998. A change detection experiment using vegetation indices. Photogrammetric Engineering and Remote Sensing 64 (2), 143–150.

Marsh, S., Walsh, J., Lee, C., Beck, L., Hutchinson, C., 1992. Comparison of multi-temporal NOAA-AVHRR and SPOT XS satellite data for mapping land cover dynamics in the west African Sahel. International Journal of Remote Sensing 13, 2997–3016.

Martin, M.P., Chuvieco, E., 1995. Mapping and evaluation of burnt land from multi-temporal analysis of AVHRR NDVI images. EARSEL Advance Remote Sensing 4, 7–13.

Miller, J.D., Yool, S.R., 2002. Mapping forest post-fire canopy consumption in several overstory types using multi-temporal Landsat TM and ETM data. Remote Sensing of Environment 82, 481–496.

Pereira, J.M.C., 1999. A comparative evaluation of NOAA/AVHRR vegetation indexes for burned surface detection and mapping. IEEE Transactions on Geoscience and Remote Sensing 37, 217–226.

Pu, R., Gong, P., 2004. Determination of burnt scars using logistic regression and neural network techniques from single post-fire Landsat 7 ETM+ image. Photogrammetric Engineering and Remote Sensing 70 (7), 841–850.

Quintano, C., Fernandez-Manso, A., Fernandez-Manso, O., Shimabukuro, Y.E., 2006. Mapping burned areas in Mediterranean countries using spectral mixture analysis from a uni-temporal perspective. International Journal of Remote Sensing 27 (4), 645–662.

Rogan, J., Yool, S., 2001. Mapping fire induced vegetation depletion in the Peloncillo Mountains, Arizona and New Mexico. International Journal of Remote Sensing 22 (16), 3101–3121.

Roy, D.R., Boschetti, L., Trigg, S.N., 2006. Remote sensing of fire severity: assessing the performance of the normalized burn ratio. IEEE Geoscience and Remote Sensing Letters 3 (1), 112–116.

Rouse Jr., J., Haas, R., Deering, D.W., Schell, J., Harlan, J., 1974. Monitoring the vernal advancement and retrogradation (Green Wave Effect) of natural vegetation, NASA/GSFC Type III Final Report, Greenbelt, MD, 371.

Sa, A.C.L., Pereira, J.M.C., Vasconcellos, M.J.P., Silva, J.M.N., Ribeiro, N., Awasse, A., 2003. Assessing the feasibility of sub-pixel burned area mapping in miombo woodlands of northern Mozambique using MODIS imagery. International Journal of Remote Sensing 24, 1783–1796.

Saunders, R.W., 1990. The determination of broad band surface albedo from AVHRR visible and near-infrared radiances. International Journal of Remote Sensing 11 (January (1)), 49–67.

Sifakis, N., Paronis, D., Keramitsoglou, I., 2004. An application of AVHRR imagery used in combination with CORINE Land Cover data for forest-fire observations and consequences assessment. International Journal of Applied Earth Observation and Geoinformation 5 (4), 263–274.

Simard, M., Saatchi, S.S., De Grandi, G., 2000. The use of decision tree and multi-scale texture for classification of JERS-1 SAR data over Tropical forest. IEEE Transactions on Geoscience and Remote Sensing 38 (5), 2310–2321.

Tappan, G., Tyler, D., Wehde, M., Moore, D., 1992. Monitoring rangeland dynamics in Senegal with advanced very high resolution radiometer data. Geocarto International 1, 87–98.

Ustin, S.L., 2004. Manual of Remote Sensing, Vol.4, Remote Sensing for Natural Resource Management and Environmental Monitoring. Wiley, New Jersey, 736 pp.

Vafeidis, A.T., Drake, N.A., 2005. A two-step method for estimating the extent of burnt areas with the use of coarse-resolution data. International Journal of Remote Sensing 26 (11), 2441–2459.

Verhoef, W., 1984. Light scattering by leaf layers with application to canopy reflectance modelling: the SAIL model. Remote Sensing of Environment 16, 125–141.

Verhoef, W., 1985. Earth observation modelling based on layer scattering matrices. Remote Sensing of Environment 17, 165–178.

Verhoef, W., Bach, H., 2003. Simulation of hyperspectral and directional radiance images using coupled biophysical and atmospheric radiative transfer models. Remote Sensing of Environment 87, 23–41.